

AN EXTREMELY LUMINOUS AND VARIABLE ULTRALUMINOUS X-RAY SOURCE IN THE OUTSKIRTS OF CIRCINUS OBSERVED WITH *NuSTAR*

D. J. WALTON¹, F. FUERST¹, F. A. HARRISON¹, D. STERN^{1,2}, M. BACHETTI^{3,4}, D. BARRET^{3,4}, F. E. BAUER^{5,6}, S. E. BOGGS⁷, F. E. CHRISTENSEN⁸, W. W. CRAIG^{7,9}, A. C. FABIAN¹⁰, B. W. GREFENSTETTE¹, C. J. HAILEY¹¹, K. K. MADSEN¹, J. M. MILLER¹², A. PTAK¹³, V. RANA¹, N. A. WEBB^{3,4}, W. W. ZHANG¹³

¹Space Radiation Laboratory, California Institute of Technology, Pasadena, CA 91125, USA

²Jet Propulsion Laboratory, California Institute of Technology, Pasadena, CA 91109, USA

³Universite de Toulouse; UPS-OMP; IRAP; Toulouse, France

⁴CNRS; IRAP; 9 Av. colonel Roche, BP 44346, F-31028 Toulouse cedex 4, France

⁵Instituto de Astrofísica, Facultad de Física, Pontificia Universidad Católica de Chile, 306, Santiago 22, Chile

⁶Space Science Institute, 4750 Walnut Street, Suite 205, Boulder, Colorado 80301

⁷Space Sciences Laboratory, University of California, Berkeley, CA 94720, USA

⁸DTU Space, National Space Institute, Technical University of Denmark, Elektrovej 327, DK-2800 Lyngby, Denmark

⁹Lawrence Livermore National Laboratory, Livermore, CA 94550, USA

¹⁰Institute of Astronomy, University of Cambridge, Madingley Road, Cambridge CB3 0HA, UK

¹¹Columbia Astrophysics Laboratory, Columbia University, New York, NY 10027, USA

¹²Department of Astronomy, University of Michigan, 500 Church Street, Ann Arbor, MI 48109-1042, USA

¹³NASA Goddard Space Flight Center, Greenbelt, MD 20771, USA

Draft version October 11, 2013

ABSTRACT

Following a serendipitous detection with the *NuSTAR* observatory, we present a multi-epoch spectral and temporal analysis of an extremely bright ultraluminous X-ray source (ULX) located in the outskirts of the Circinus galaxy ($\sim 4'$ away from the nucleus), hereafter Circinus ULX5, including coordinated follow-up observations with *XMM-Newton* and *NuSTAR*. The *NuSTAR* data presented here represent one of the first instances of a ULX reliably detected at hard ($E > 10$ keV) X-rays. Circinus ULX5 is variable on long timescales by at least a factor of ~ 5 in flux, and was caught in a historically bright state during our 2013 observations, with an observed 0.3–30.0 keV luminosity of 1.6×10^{40} erg s⁻¹. During this epoch, the source displayed a curved 3–10 keV spectrum, broadly similar to other bright ULXs. Although pure thermal models result in a high energy excess in the *NuSTAR* data, this excess is too weak to be modelled with the disk reflection interpretation previously proposed to explain the 3–10 keV curvature in other ULXs. In addition to flux variability, Circinus ULX5 also displays clear spectral variability. While in many cases the interpretation of spectral components in ULXs is uncertain, the spectral and temporal properties of the all the high quality datasets currently available strongly support a simple disk–corona model reminiscent of that invoked for Galactic binaries, with the accretion disk becoming more prominent as the luminosity increases. However, although the disk temperature and luminosity are remarkably well correlated across all timescales currently probed, the observed relation is $L \propto T^{1.70 \pm 0.17}$, flatter than that expected for simple blackbody radiation. The spectral variability displayed by Circinus ULX5 is highly reminiscent of that observed from the Galactic black hole binaries (BHBs) XTE J1550-564 and GRO J1655-40 at high luminosities. This comparison would imply a black hole mass of $\sim 90 M_{\odot}$ for Circinus ULX5. However, given the diverse behavior observed from Galactic BHB accretion disks, this mass estimate is still uncertain. Finally, during our coordinated *XMM-Newton*+*NuSTAR* observation we find no evidence for any ionised iron absorption lines, typically associated with disk winds in Galactic BHBs. The limits placed on any undetected features imply that we are not viewing the central regions of Circinus ULX5 through any extreme super-Eddington outflow.

Subject headings: Black hole physics, X-rays: binaries, X-rays: individual (Circinus ULX5)

1. INTRODUCTION

The origin of the extreme luminosities displayed by ultraluminous X-ray sources (ULXs; $L_X \gtrsim 10^{39}$ erg s⁻¹) may relate to exotic super-Eddington modes of accretion (*e.g.* Poutanen et al. 2007, Finke & Böttcher 2007), or alternatively to the presence of black holes larger than typically found in Galactic black hole binary systems (BHBs; $M_{\text{BH}} \sim 10 M_{\odot}$), potentially the long sought intermediate mass black holes (IMBHs: $10^2 \lesssim M_{\text{BH}} \lesssim 10^5 M_{\odot}$; *e.g.* Miller et al. 2004; Strohmayr 2009). For recent reviews see Roberts (2007) and Feng & Soria (2011).

The majority of ULXs only modestly exceed 10^{39} erg s⁻¹, and therefore likely represent a natural extension of the disk–

dominated high-Eddington thermal states displayed by Galactic BHBs (*e.g.* Kajava & Poutanen 2009; Middleton et al. 2013). However, a much smaller fraction of the ULX population have been observed to exceed 10^{40} erg s⁻¹ in X-rays (Walton et al. 2011b; Jonker et al. 2012; Sutton et al. 2012), and in the most luminous case known to date to reach as high as $\sim 10^{42}$ erg s⁻¹ (Farrell et al. 2009). These more luminous sources, apparently radiating in excess of 10 times the Eddington limit for a $10 M_{\odot}$ black hole, remain among the best known candidates to host massive black holes.

Here we report on an extremely bright and highly variable ULX in the outskirts of the Circinus galaxy ($z = 0.001448$, $D \sim 4$ Mpc; Freeman et al. 1977; Koribalski et al.

2004), hereafter Circinus ULX5 (there are up to four other known/claimed ULX candidates closer to the Circinus nucleus, see *e.g.* Bauer et al. 2001; Swartz et al. 2004; Liu & Mirabel 2005; Ptak et al. 2006). Circinus ULX5 was serendipitously detected in a high luminosity state by *NuSTAR* on 25th Jan 2013, and we subsequently performed follow-up target-of-opportunity (ToO) observations with both *XMM-Newton* and the recently launched Nuclear Spectroscopic Telescope Array (*NuSTAR*; Harrison et al. 2013). In spite of its luminosity, Circinus ULX5 has received little attention to date, owing in large part to its fairly substantial separation from the galaxy centre (Circinus ULX5 formally falls outside the D25 isophote for Circinus). The only mention of the source is in the Winter et al. (2006) ULX catalogue.¹ In section 2 we detail our data reduction procedure for the various datasets considered, and in sections 3, 4 and 5 we describe our multi-epoch spectral and temporal analysis of this remarkable source. Key results are discussed in section 6, and we summarise our conclusions in section 7. Throughout this work, we will assume Circinus ULX5 is indeed associated with the Circinus galaxy. Possible alternative scenarios are discussed in section 6.1, but we consider them highly unlikely.

2. DATA REDUCTION

Here we outline our data reduction procedure for the X-ray observations considered in this work, beginning with the new *XMM-Newton* and *NuSTAR* datasets obtained in early 2013.

2.1. 2013 Observations

2.1.1. *NuSTAR*

NuSTAR (Harrison et al. 2013) performed four observations of the Circinus field throughout late January and early February 2013. The first observation, in which the bright ULX was serendipitously detected, was optimized to observe the galaxy’s nucleus, but the three subsequent follow-up observations were all optimized to observe the ULX, which is offset from the nucleus by $\sim 4'$ (see Fig. 1): RA = $14^h 12^m 39^s$, DEC = $-65^\circ 23' 34''$. The data have been reduced using the standard pipeline, part of the *NuSTAR* Data Analysis Software v0.11.1 (NUSTARDAS, part of the standard HEASOFT distribution as of version 14), and instrumental responses from *NuSTAR* caldb² v20130509 are used throughout. As discussed in Risaliti et al. (2013), these responses have been empirically corrected such that the Crab nebula gives a powerlaw spectrum with a photon index of $\Gamma_{\text{Crab}} = 2.1$. Full details are provided in Madsen et al. 2013 (*in prep.*), but the calibration has also been successfully tested against other powerlaw-like sources, including the pulsar wind nebula G 21.5-0.9 and the blazar PKS 2155, which are frequently used to assess the calibration of X-ray missions (Tsujimoto et al. 2011; Ishida et al. 2011). The unfiltered event files have been cleaned with the standard depth correction, which significantly reduces the internal background at high energies, and SAA passages have been removed. Source products were obtained from circular regions of $\sim 70''$ in radius for the observations with the ULX on the optical axis, and $\sim 50''$ in radius for the initial detection to avoid the edge of the detector, and background was estimated from a blank area of the same detector free from

¹ Note that in Winter et al. (2006), the source studied here is referred to as Circinus XMM2.

² The *NuSTAR* calibration database is available through HEASARC: <http://heasarc.gsfc.nasa.gov/docs/heasarc/caldb/nustar>

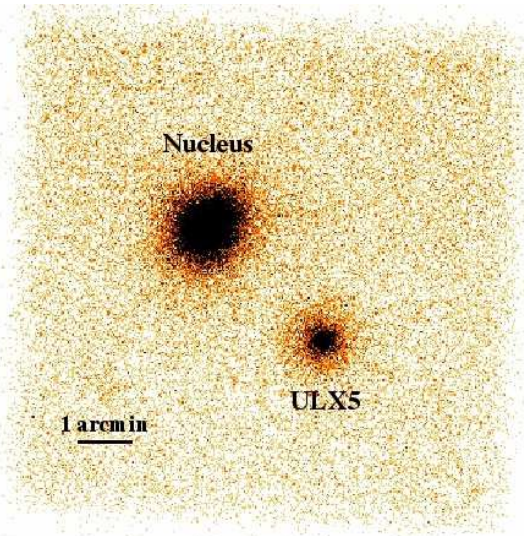


FIG. 1.— *NuSTAR* FPMA image of the Circinus field. The Circinus nucleus and Circinus ULX5, separated by $\sim 4'$, are both highlighted.

contaminating point sources. Spectra and lightcurves were extracted from the cleaned event files using XSELECT for both focal plane modules (FPMA and FPMB). Finally, the spectra were grouped with GRPPHA such that each spectral bin contains at least 50 counts. Although *NuSTAR* operates over the 3-79 keV energy range, Circinus ULX5 is only reliably detected up to ~ 30 keV.

2.1.2. *XMM-Newton*

After the initial serendipitous *NuSTAR* detection, we also triggered a ~ 50 ks target-of-opportunity (ToO) observation with *XMM-Newton* (Jansen et al. 2001) in order to provide complimentary soft X-ray coverage for our targeted *NuSTAR* follow-up observations (performed simultaneously with *NuSTAR* obsid 30002038004). Data reduction was carried out with the *XMM-Newton* Science Analysis System (SASv12.0.1) largely according to the standard prescription provided in the online guide.³ The observation data files were processed using EPCHAIN and EMCHAIN to produce calibrated event lists for the *EPIC*-pn (Strüder et al. 2001) and *EPIC*-MOS (Turner et al. 2001) detectors, respectively. For each detector, source products were extracted from a circular region of $\sim 40''$ in radius, and background was estimated from an area of the same CCD free of contaminating point sources. Lightcurves and spectra were generated with XMMSELECT, selecting only single and double events (single to quadruple events) for *EPIC*-pn (*EPIC*-MOS), excluding periods of high background flares (occurring predominantly at the end of the observation). The redistribution matrices and auxiliary response files were generated with RMFGEN and ARFGEN, while lightcurves were corrected for the background count rate using EPICLCCORR. After performing the data reduction separately for each of the MOS CCDs and confirming their consistency, the spectra were combined using the FTOOL ADDASCASPEC. Finally, spectra were re-binned to have a minimum of 50 counts in each energy bin, and analysed across the full 0.3–10.0 keV energy range.

³ <http://xmm.esac.esa.int/>

TABLE 1
 DETAILS OF THE X-RAY OBSERVATIONS CONSIDERED IN THIS WORK, ORDERED CHRONOLOGICALLY.

Mission	OBSID	Date	Target	Good Exposure (ks)	ULX5 3-10 keV Flux ^b (10^{-12} erg cm ⁻² s ⁻¹)
<i>XMM-Newton</i>	0111240101	2001-08-06	Nucleus	105/110/ ^a	1.09 ± 0.04
<i>Suzaku</i>	701036010	2006-07-21	Nucleus	110	1.55 ± 0.04
<i>Swift</i>	00035876001	2007-03-23	Field	7.5	0.8 ^{+0.1} _{-0.3}
<i>Swift</i>	00037273001	2008-05-18	Field	6	1.0 ^{+0.3} _{-0.4}
<i>Chandra</i>	10873	2009-03-01	SN1996cr	18	5.0 ± 0.5
<i>Chandra</i>	10850	2009-03-03	SN1996cr	14	4.8 ^{+0.4} _{-0.5}
<i>Chandra</i>	10872	2009-03-04	SN1996cr	17	1.0 ^{+0.2} _{-0.1}
<i>Swift</i>	00090260001	2009-11-15	Field	5	2.3 ^{+1.0} _{-0.6}
<i>Swift</i>	00037273004	2012-11-11	Field	3.5	1.0 ^{+0.7} _{-0.5}
<i>NuSTAR</i>	60002039002	2013-01-25	Nucleus	55	4.2 ± 0.2
<i>Swift</i>	00032699001	2013-01-31	Field	3.5	5.0 ^{+1.3} _{-1.0}
<i>NuSTAR</i>	30002038002	2013-02-02	ULX5	18	4.2 ± 0.2
<i>XMM-Newton</i>	0701981001	2013-02-03	ULX5	37/47/47 ^a	(as below)
<i>NuSTAR</i>	30002038004	2013-02-03	ULX5	40	4.93 ± 0.12
<i>NuSTAR</i>	30002038006	2013-02-05	ULX5	36	3.7 ± 0.1

^a *XMM-Newton* exposures are listed for the *EPIC*-pn/MOS1/MOS2 detectors.

^b Observed fluxes are computed in sections 3 for the higher S/N observations, utilizing the DISKBB+SIMPL model, and in 5.1 for the shorter shapshot observations, utilizing a simpler cutoff-powerlaw model.

2.2. Archival Data

Prompted by the new data obtained in 2013, we also searched the X-ray archive for observations of the Circinus field, in order to investigate potential long term variability. A summary of all the X-ray observations considered in this work is given in Table 1. The additional archival observations were almost all targeted at the Circinus nucleus or the nearby supernova SN1996cr (Bauer et al. 2008), but Circinus ULX5 is serendipitously included in the field-of-view, albeit substantially off-axis, in each case.

2.2.1. *XMM-Newton*

In addition to the recent ToO we obtained, *XMM-Newton* also observed Circinus in August 2001. This observation was largely reduced in the same manner as the ToO described above (section 2.1.2). However, in this case the target was the Circinus nucleus, and the ULX in question unfortunately fell very close to a chip gap in the *EPIC*-pn detector. Furthermore, the MOS2 detector was operated in partial window mode, and the target fell outside the operational region of the detector. In this case, we use an elliptical source region for *EPIC*-pn, offset slightly from the source position in order to include as many counts as possible without the region covering the chip gap. The shape of the *EPIC*-pn spectrum obtained is consistent with that obtained with MOS1, however we do find that the flux normalisation is not consistent between the detectors. We therefore take the MOS1 detector as the true flux indicator for this observation, given the non-standard reduction necessary for *EPIC*-pn. In this case, as the average countrate is much lower than the more recent *XMM-Newton* observation, owing to the combined effect of a large off-axis angle and a lower source flux (see section 3.3 and Table 1), we rebin instead to a minimum of 25 counts per bin.

2.2.2. *Suzaku*

The Circinus field was also observed by *Suzaku* (Mitsuda et al. 2007) in July 2006. Owing to the obvious, dominant contribution from the nucleus, we do not consider the HXD detectors in this work, and focus instead on the data obtained with the XIS CCDs. Following the recommendation in the *Suzaku* Data Reduction Guide,⁴ we reprocessed the unfiltered event files for each of the operational XIS detectors (XIS0, 1, 2 and 3; Koyama et al. 2007) and editing modes (3x3 and 5x5) using the latest HEASOFT software package (v6.13). Cleaned event files were generated by re-running the *Suzaku* pipeline with the latest calibration, as well as the associated screening criteria files. Source products were extracted from a circular region of $\sim 85''$ in radius, in order to avoid contamination from a further faint source nearby (separated by $\sim 105''$), and the background was extracted from regions free of any obvious contaminating point sources, but close to the source region. Spectra and lightcurves were extracted from the cleaned event files with XSELECT, and responses were generated for each detector using the XISRESP script with a medium resolution. The spectra and response files for the front-illuminated detectors (XIS0, 2 and 3) were combined using the FTOOL ADDASCASPEC, after confirming their consistency. Finally, we again grouped the spectra to have a minimum of 50 counts per energy bin. In this work, we analyse the XIS data over the 0.5–10.0 keV energy range.

2.2.3. *Chandra*

Although the Circinus field has also frequently been observed by the *Chandra* X-ray observatory (Weisskopf et al. 2002), Circinus ULX5 only fell in the field-of-view for three of these pointings (see Table 1). For each of the three ob-

⁴ <http://heasarc.gsfc.nasa.gov/docs/suzaku/analysis/>

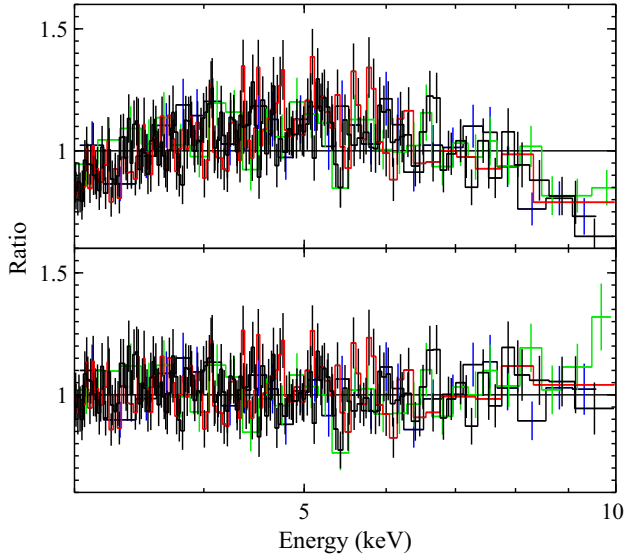


FIG. 2.— Data/model ratios for the simultaneous *XMM-Newton* (black: *EPIC-pn*, red: *EPIC-MOS*) and *NuSTAR* (green: *FPMA*, blue: *FPMB*) datasets, modelled with both a powerlaw continuum modified by Galactic absorption (*top panel*) and an unabsorbed disk component (*bottom panel*). The *XMM-Newton* and *NuSTAR* datasets display clear and consistent curvature across their common energy range (3–10 keV).

servations, the instrument was operated in the Timed Event mode, and we extracted spectra from the ACIS-S detector (Garmire et al. 2003) using the standard pipeline CIAO v4.5. In all observations Circinus ULX5 is detected close to the edge of the field of view, while the observatory pointed at SN1996cr. At these large off-axis angles the *Chandra* PSF is clearly elongated, so we used an elliptical extraction region with major and minor axes of $5.5 \times 2.7''$ to gather all source photons. The background was extracted from two large circular regions above and below the HETG diffraction pattern, free from any other contaminating sources. The *Chandra* spectra were rebinned to a signal-to-noise ratio (S/N) of 2, and modelled over the full 0.3–9.0 keV energy range.

2.2.4. *Swift* Snapshots

Finally, *Swift* (Gehrels et al. 2004) has also sporadically taken snapshot observations of the Circinus field. We searched the *Swift* archive for pointed observations with at least 1 ks duration, such that reasonable flux estimates might be obtained, and found 5 observations that met our criteria. Cleaned event files were generated in the standard manner with XRTPIPELINE, and spectral products were extracted with XSELECT. Source spectra were taken from circular regions of radius $\sim 30''$, and background spectra from larger, adjacent regions free of contaminating point sources. Ancilliary responses were generated with XRTMKARF, and we use the latest redistribution matrices available in the *Swift* calibration database (v13). The *Swift* spectra were only grouped to have at least 5 counts per spectral bin, such that even the observations with the lowest S/N (OBSIDs 00037273001 and 00037273004) had at least 10 spectral bins across the 0.3–10.0 keV energy range.

3. SPECTRAL ANALYSIS

The majority of our spectral analysis focuses on the long, higher S/N observations of the ULX, *i.e.* the joint 2013 *XMM-Newton* and *NuSTAR* dataset, the 2006 *Suzaku* data and the 2001 *XMM-Newton* data. Throughout this work, spectral

modelling is performed with XSPEC v12.8.0 (Arnaud 1996), and quoted uncertainties on spectral parameters are the 90 per cent confidence limits for a single parameter of interest, unless stated otherwise. Unless stated otherwise, spectral fitting is performed through χ^2 minimisation. Neutral absorption is treated with TBNEW⁵, the latest version of the TBABS absorption code (Wilms et al. 2000), with the appropriate solar abundances. Unless stated otherwise, all models include Galactic absorption with a column of $N_{\text{H,Gal}} = 5.58 \times 10^{21} \text{ cm}^{-2}$ (Kalberla et al. 2005). In the following, data from a variety of X-ray missions are utilised, many of which operate multiple detectors simultaneously (*e.g.* *EPIC-pn* and *EPIC-MOS* aboard *XMM-Newton*). In these cases, the data from the different detectors are modeled simultaneously, with all parameters tied between the spectra. However, we attempt to account for any residual internal cross-calibration uncertainties between the detectors by including a variable multiplicative cross-normalisation constant. This value is almost always found to be within ~ 5 per cent of unity for all such missions, with the only exception being the 2001 *XMM-Newton* data, owing to the unfortunate position of the source on the *EPIC-pn* detector as discussed previously (see section 2.2.1).

3.1. *NuSTAR* and *XMM-Newton* in 2013

3.1.1. Cross-Calibration

We begin our analysis with the recent broadband *XMM-Newton*+*NuSTAR* spectrum. When modeling this joint dataset, we treat possible issues with flux cross-calibration between *NuSTAR* and *XMM-Newton* in the same way as we do cross-calibration uncertainties between different detectors within a single mission (see above). The individual *NuSTAR* and *XMM-Newton* datasets have substantial spectral overlap, both covering the 3–10 keV energy range, from which cross-normalisation constants can easily be constrained. In order to demonstrate the spectral consistency between *XMM-Newton* and *NuSTAR*, we initially focus on this energy range.

Applying a simple powerlaw model, modified by Galactic absorption results in a poor fit, with $\chi^2_{\nu} = 796/565$ and clear curvature present in the residuals for both the *XMM-Newton* and *NuSTAR* data (Fig. 2, *upper panel*). Inspection of the full 0.3–10.0 keV *XMM-Newton* data suggests the overall neutral column is most likely in excess of the Galactic column, closer to $N_{\text{H,tot}} \sim 10^{22} \text{ atom cm}^{-2}$, but even allowing for a column of this order does not fully remove the curvature in the 3–10 keV bandpass (a total column of $N_{\text{H,tot}} \sim 10^{22} \text{ atom cm}^{-2}$ still has a very limited effect above 3 keV). We therefore conclude that the 3–10 keV continuum of Circinus ULX5 is intrinsically curved, similar to other bright ULXs (Stobbart et al. 2006; Gladstone et al. 2009; Walton et al. 2011a). If we instead model the 3–10 keV data with a curved continuum, simply parameterising the data with an unabsorbed DISKBB component (Mitsuda et al. 1984), we obtain an excellent fit with $\chi^2_{\nu} = 563/564$ (Fig. 2, *lower panel*). Allowing the *XMM-Newton* and *NuSTAR* temperatures to vary independently does not improve the fit at all ($\chi^2_{\nu} = 563/563$), and we obtain $T_{\text{XMM}} = 2.01 \pm 0.04 \text{ keV}$ and $T_{\text{NuSTAR}} = 2.04 \pm 0.06 \text{ keV}$. Clearly the 3–10 keV spectra obtained with *XMM-Newton* and *NuSTAR* are fully consistent. Furthermore, the *NuSTAR* and *EPIC-MOS* fluxes agree to within $\sim 15\%$.

⁵ <http://pulsar.sternwarte.uni-erlangen.de/wilms/research/tbabs>

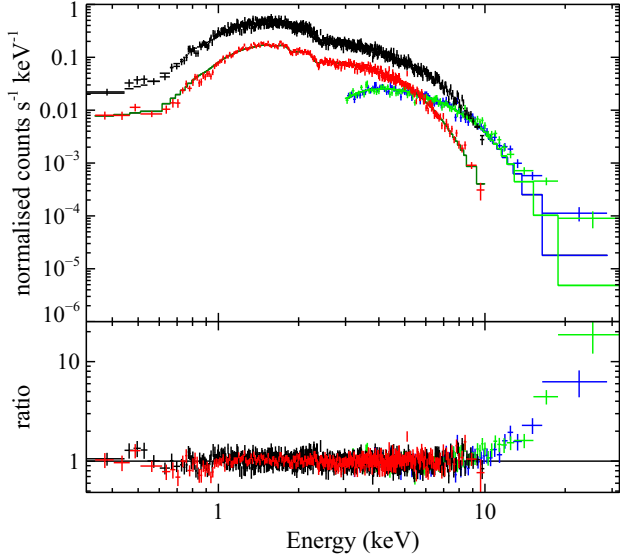


FIG. 3.— The broadband 0.3–30.0 keV spectrum of Circinus ULX5 modelled with a simple DISKBB accretion disk model. This model results in a clear excess in the *NuSTAR* data above 10 keV.

3.1.2. Continuum Modelling

We now consider the full 0.3–30.0 keV broadband spectrum, and model the *XMM-Newton* and *NuSTAR* data simultaneously. In addition, we now (and hereafter) formally include both Galactic absorption and intrinsic neutral absorption (at the redshift of Circinus), the latter being free to vary. Naturally, the simple powerlaw continuum continues to provide a very poor fit ($\chi^2_\nu = 3388/1119$). However, applying the simple accretion disk continuum also results in a fairly poor fit ($\chi^2_\nu = 1287/1119$), and clear divergence between the data and the model can be seen in the residuals at high energies ($\gtrsim 10$ keV; see Fig. 3), where the Wien tail of the DISKBB model falls away far faster than the data.

Initially, we attempt to model this additional high energy emission with a powerlaw-like Comptonised component, applying the SIMPL convolution model (Steiner et al. 2009), which ‘scatters’ some fraction of an input seed photon distribution into a high energy powerlaw tail, to the DISKBB continuum. We use this model rather than a basic powerlaw component in order to ensure that the powerlaw does not extrapolate to arbitrarily low energies, which is potentially important given the high temperature of the disk (~ 2 keV). SIMPL has three parameters, the photon index of the high energy tail, the fraction of the seed flux scattered into the high energy tail (f_{scat}), and a flag determining whether to allow for both Compton up- and down-scattering, or just the former. For simplicity, we only allow for up-scattering of the seed photon spectrum, although the results obtained are not sensitive to this assumption. The addition of this component significantly improves the fit, with $\chi^2_\nu = 1137/1117$, *i.e.* an improvement of $\Delta\chi^2 = 150$ for two additional free parameters, and resolves the excess at high energies. The parameter values obtained are quoted in Table 2. However, a number of parameters are found to be degenerate with one another; this is particularly the case for the parameters that determine the high energy spectrum (see Fig. 4). Although fairly poorly constrained owing to these degeneracies, the photon index obtained is very steep, $\Gamma = 4.0^{+0.4}_{-0.8}$.

The full 0.3–30.0 keV observed flux from Circinus ULX5 during this epoch is $(8.5 \pm 0.3) \times 10^{-12}$ erg cm $^{-2}$ s $^{-1}$. Owing

to the steep high energy spectrum, this is mostly dominated by the emission below 10 keV, which contributes 85 per cent of the total 0.3–30.0 keV flux. At the distance of Circinus ($D \sim 4$ Mpc; Freeman et al. 1977; Koribalski et al. 2004), the broadband flux corresponds to an extreme luminosity of $L_{0.3-30.0} = (1.63 \pm 0.06) \times 10^{40}$ erg s $^{-1}$, assuming isotropic emission, placing Circinus ULX5 amongst the most luminous ULXs known to date, even before absorption corrections are considered. Although the exact correction is somewhat model dependent, for the DISKBB+SIMPL combination, the intrinsic 0.3–30.0 keV luminosity inferred is $\sim 2 \times 10^{40}$ erg s $^{-1}$, a further ~ 20 per cent larger than the observed luminosity.

Given the steep nature of the high energy spectrum, it is not clear that the hard excess can be considered to be similar to the hard excesses frequently seen in AGN (*e.g.* Walton et al. 2010, 2013b; Nardini et al. 2011; Risaliti et al. 2013; Rivers et al. 2013) and BHBs (*e.g.* Zdziarski et al. 2002; Corongiu et al. 2003; Reis et al. 2010), which are best associated with Compton reflection (and if phenomenologically modeled with a powerlaw would generally give $\Gamma \ll 2$). It has recently been suggested that the combination of iron emission and absorption in a relativistically smeared reflection spectrum from the inner regions of the accretion disc might be able to explain the curvature observed below 10 keV in bright ULXs (Caballero-García & Fabian 2010). This would then allow the intrinsic high energy emission to have a powerlaw-like form, as is typical for sub-Eddington coronal emission. In general, this interpretation required high iron abundances and strong relativistic broadening in order to reproduce the smooth 3–10 keV curvature (Caballero-García & Fabian 2010; Walton et al. 2011a). However, while such a model, consisting of a powerlaw-like corona and a smeared reflection component (modelled with a combination of the REFLIONX reflection code, Ross & Fabian 2005, and the RELCONV relativistic kernel, Dauser et al. 2010) does provide an adequate fit to the *XMM-Newton* data alone ($\chi^2_\nu = 1018/950$), when fit to the broadband spectrum the Compton reflection hump at ~ 20 keV is significantly in excess of the observed *NuSTAR* data, as is clear from Fig. 5 (see also Walton et al. 2011a), and the resulting fit is rather poor ($\chi^2_\nu = 1623/1111$).

In this case, however, there is formally an alternative solution using this model combination that provides an acceptable fit to the broadband spectrum ($\chi^2_\nu = 1145/1113$), although it is rather different than previous applications to ULXs. Rather than model the curvature with iron emission/absorption, this fit instead attempts to remove all iron features, and requires the lowest iron abundance allowed by the model.⁶ Without any iron absorption at ~ 7 keV, the peak of the Compton hump shifts to lower energies. In addition, the spin obtained is very high, the radial emissivity index is maximized, the disk is required to be face on, and its ionisation state is minimized. This combination serves to further reduce the energy of the peak of the Compton hump, to the extent that the 3–10 keV curvature is actually modelled by this aspect of the reflected emission. In fact, in this extreme corner of parameter space, the reflection component is smeared and shifted to such an extent that, when absorbed by a substantial neutral column, it takes on the appearance of a hot thermal-like spectrum with a steep powerlaw tail. All the features typically associated with reflected

⁶ The REFLIONX grid utilised is calculated for photon indices in the range $\Gamma = 1.4-3.3$, ionisation states in the range $\log \xi = 0-4$, and iron abundances in the range 0.1–10.0.

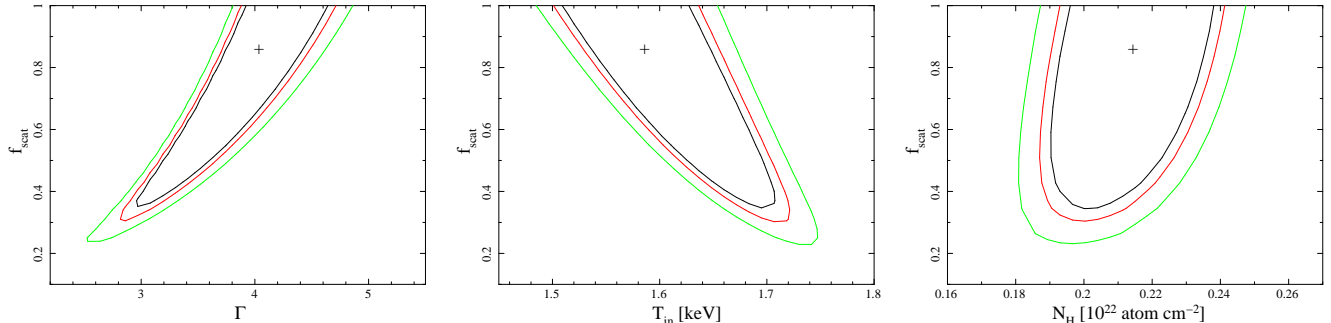


FIG. 4.— Two-dimensional χ^2 confidence contours for various parameter combinations from the DISKBB+SIMPL model: the photon index (Γ), disk temperature (T_{in}) and the intrinsic neutral column (N_{H}) are each paired with the fraction of the diskbb flux scattered into the high energy tail (f_{scat}) in the *left*, *centre* and *right* panels respectively. In each case the black, red and green contours show the 90, 95, and 99% confidence intervals (for 2 parameters of interest). Fairly strong parameter degeneracies are observed in some cases.

emission are essentially removed, which we interpret as further evidence that the spectrum of Circinus ULX5 is not well modelled with traditional disc reflection. Therefore, although statistically acceptable, we consider this to be a very unsatisfying solution. If reflection is a relevant process for ULXs, the picture must be more complex than the standard thin disk–corona accretion geometry. Owing to the complexity of the model, we do not include the results obtained in Table 2.

If ULXs do represent a population of sources accreting at very high- or super-Eddington rates, the expected emission from the accretion disc may in fact be substantially different from the simple Shakura & Sunyaev (1973) thin disc profile assumed in the DISKBB model. As the accretion rate increases towards substantial Eddington fractions, the scale height of the disc is expected to increase, and advection becomes an increasingly important process (Abramowicz et al. 1988), resulting in shallower radial temperature profiles and hence giving the appearance of a broader, less-peaked emission profile from the disc. In order to investigate whether a broader disc profile could potentially account for the additional hard emission relative to the simple DISKBB profile, we attempted to model the broadband spectrum with a DISKPBB model, which includes the index of the radial temperature profile (p) as an additional free parameter (Mineshige et al. 1994). This does offer a substantial improvement over the pure DISKBB model, with $\chi^2_{\nu} = 1181/1118$, and the radial temperature profile obtained is indeed shallower than expected for a thin disc (*i.e.* $p < 0.75$). However, as shown in Fig. 5 we again see an excess of emission over the DISKPBB model, although it is slightly weaker than in the DISKBB case, owing to the disc emission being able to extend to higher energies while still reproducing the observed curvature in the 3–10 keV bandpass. An additional component is still required. In fact, this is the case for *any* model invoked to explain the curvature below 10 keV that falls away above 10 keV with a thermal Wien spectrum, including more detailed accretion disc models (*e.g.* KERRBB; Li et al. 2005) and optically thick Comptonisation by cool (~ 2 keV) electrons (*e.g.* Gladstone et al. 2009).

Adding a Comptonised component (SIMPL) to the DISKPBB model again provides a clear improvement to the fit, with $\chi^2_{\nu} = 1131/1116$, *i.e.* an improvement of $\Delta\chi^2 = 50$ for two additional free parameters over the pure DISKPBB model. However, the improvement over the DISKBB+SIMPL combination is very marginal, $\Delta\chi^2 = 6$ for one additional free parameter, and the additional model complexity serves to further exacerbate the parameter degeneracies already present

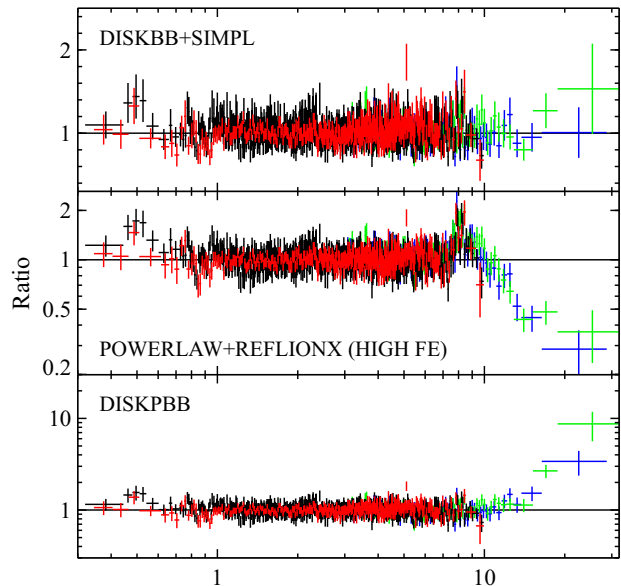


FIG. 5.— Data/model ratios for a selection of the models applied to the combined *XMM-Newton*+*NuSTAR* dataset for Circinus ULX5 (see text for details). *Top panel*: the DISKBB+SIMPL combination, which provides an excellent fit to the broadband spectrum. *Middle panel*: the relativistic disk reflection model in which the 3–10 keV curvature is modelled as blurred iron emission/absorption (the high iron abundance fit), which severely overpredicts the high energy *NuSTAR* data. *Bottom panel*: the DISKPBB model, which still underpredicts the high energy data, similar to the simpler DISKBB model.

with the DISKBB+SIMPL model (Fig. 4). The best fit radial temperature profile for the disc is only marginally constrained to be shallower than expected for the thin disc case ($p = 0.67^{+0.05}_{-0.02}$), and in this instance we find that the photon index is only loosely constrained at all ($\Gamma < 3.9$).

For completeness, we also fit the DISKBB+COMPTT combination, frequently used to parameterise the spectra from bright ULXs (*e.g.* Gladstone et al. 2009; Middleton et al. 2011; Walton et al. 2011a, 2012a), which allows for a variable electron temperature for the thermal Comptonisation (Titarchuk 1994). Unsurprisingly, this also provides an excellent fit ($\chi^2_{\nu} = 1140/1114$), although again the additional model complexity does not offer any substantial improvement; the same model combination with the electron temperature fixed at 500 keV, such that in the *NuSTAR* band the COMPTT component is largely powerlaw-like, provides an equally good fit ($\chi^2_{\nu} = 1142/1115$). There is again substan-

TABLE 2
 BEST FIT PARAMETERS OBTAINED FOR THE VARIETY OF CONTINUUM MODELS APPLIED TO THE HIGH S/N DATA AVAILABLE FOR CIRCINUS ULX5.

Model	$N_{\text{H,int}}$ (10^{21} atom cm^{-2})	T_{in} (keV)	p	Γ	f_{scat} (or $f_{\text{h}}/f_{\text{s}}$) ^a	kT_{e} (keV)	τ	χ^2_{ν} ($=\chi^2/\text{DoF}$)
<i>XMM-Newton+NuSTAR</i> (2013)								
DISKBB	$1.6^{+0.2}_{-0.1}$	1.94 ± 0.02						1287/1119
DISKPBB	3.3 ± 0.3	2.22 ± 0.06	0.65 ± 0.01					1181/1118
DISKBB+SIMPL	2.1 ± 0.2	$1.59^{+0.09}_{-0.04}$		$4.0^{+0.4}_{-0.8}$	>0.43			1137/1117
DISKPBB+SIMPL	$3.0^{+0.3}_{-0.7}$	$2.0^{+0.1}_{-0.3}$	$0.67^{+0.05}_{-0.02}$	$<3.9^b$	$0.08^{+0.55}_{-0.03}$			1131/1116
DISKBB+COMPTT	2.1 ± 0.2	$1.5^{+0.3}_{-0.2}$			$0.38^{+0.17}_{-0.30}$	>2.8	<20	1140/1114
COMPTT ₁ +COMPTT ₂	$1.0^{+0.8}_{-0.6}$	$0.31^{+0.06}_{-0.05}$			$0.57^{+0.22}_{-0.19}$	1: $1.3^{+0.4}_{-0.2}$ 2: $3.1^{+1.2}_{-0.6}$	1: >12 2: >5	1132/1112
<i>Suzaku</i> (2006)								
POWERLAW	9.5 ± 0.5			2.46 ± 0.03				1029/618
DISKBB	$1.2^{+0.3}_{-0.2}$	1.30 ± 0.02						639/618
DISKPBB	$3.3^{+0.6}_{-0.7}$	$1.47^{+0.07}_{-0.06}$	0.61 ± 0.03					606/617
DISKBB+SIMPL	2.0 ± 0.4	$1.04^{+0.10}_{-0.08}$		$4.0^{+0.9}_{-1.9}$	>0.17			590/616
<i>XMM-Newton</i> (2001)								
POWERLAW	4.6 ± 0.4			2.18 ± 0.04				587/580
DISKBB	<0.2	$1.33^{+0.02}_{-0.03}$						820/580
DISKPBB	4.6 ± 0.4	$4.9^{+0.8}_{-0.8}$	0.483 ± 0.005					576/579
DISKBB+SIMPL	$2.0^{+0.7}_{-0.5}$	$0.6^{+0.1}_{-0.2}$		$2.2^{+0.2}_{-0.3}$	>0.55			569/578

^a For models that do not include SIMPL, hard and soft component fluxes (f_{h} and f_{s} respectively) are calculated extrapolating the model components over the energy range 0.01–100 keV. In the two COMPTT model, the higher temperature component is the harder of the two.

^b SIMPL does not allow for photon indices below ~ 1.1 .

tial degeneracy between the various physical parameters, but despite this there is a marked difference between the fit parameters for Circinus ULX5 and those obtained for other bright ($L_{\text{X}} \sim 10^{40}$ erg s^{-1}) ULXs. Here, it is the DISKBB component that primarily produces the 3–10 keV curvature, while in previous work this curvature is accounted for by the COMPTT component, resulting in cool, optically thick electron distributions being inferred. The DISKBB component instead usually accounts for the additional soft emission seen below ~ 1 keV in bright ULXs with less absorption (*e.g.* Miller et al. 2003, 2004, 2013). Unfortunately, owing to the fairly substantial total absorbing column towards Circinus ULX5, we are not highly sensitive to the presence of any such emission. In this case, the COMPTT component instead accounts for the excess emission observed above 10 keV. As such, the Comptonisation parameters are not well constrained (see Table 2). Nevertheless, the electron temperature obtained is still higher than typical results from analyses limited to below 10 keV, which find $T_{\text{e}} \sim 2$ keV, or less (*e.g.* Gladstone et al. 2009; Walton et al. 2011a).

Finally, we also consider a dual Comptonisation model for Circinus ULX5, employing two COMPTT continuum components. Such dual-coronae have been proposed for Galactic BHs in some cases (*e.g.* Makishima et al. 2008), but this is the first time such a model has been applied to a ULX. For simplicity, the seed photon temperatures for the two components are linked throughout most of our analysis. Initially, following Makishima et al. (2008), we attempted to fit the data with a common electron temperature for each COMPTT component, with the two merely having differing optical depths. However, this resulted in a relatively poor fit

($\chi^2_{\nu} = 1199/1113$), with the model failing to correctly account for the high energy emission, similar to Fig. 3. Two different electron temperatures are strongly required, as one of the components is required to model the 3–10 keV curvature, while the other needs to extend to higher energies in order to model the residual high energy excess. Allowing for two different electron temperatures, an excellent fit is obtained ($\chi^2_{\nu} = 1132/1112$). With this configuration, both electron distributions are found to be optically-thick (see Table 2), although this is no longer the case if the two components are allowed to have different seed photon temperatures, in which case the parameters of the COMPTT component that accounts for the high energy excess are only poorly constrained, as before.

3.1.3. The Iron K Region

The combined *XMM-Newton+NuSTAR* dataset has sufficient photon statistics at high energies to warrant an investigation of the iron K region (6–7 keV). Owing to their typically moderate fluxes and their frequently soft spectra, ULX datasets sensitive in the iron K energy range are naturally rare. For bright ($L_{\text{X}} > 10^{40}$ erg s^{-1}), isolated ULXs such studies have to date been limited to Holmberg IX X-1 and NGC 1313 X-1 (Walton et al. 2013a, 2012a).

To search for atomic features here, we follow the same approach undertaken in Walton et al. (2012a, 2013a). We refer the reader to those works for a detailed description of this approach, but in brief, we include a narrow (intrinsic width of $\sigma = 10$ eV) Gaussian, and vary its energy across the 5–9 keV energy range in steps of 0.04 keV. The continuum model used is the DISKBB+SIMPL combination described above. For each line energy, we record the $\Delta\chi^2$ improvement resulting from

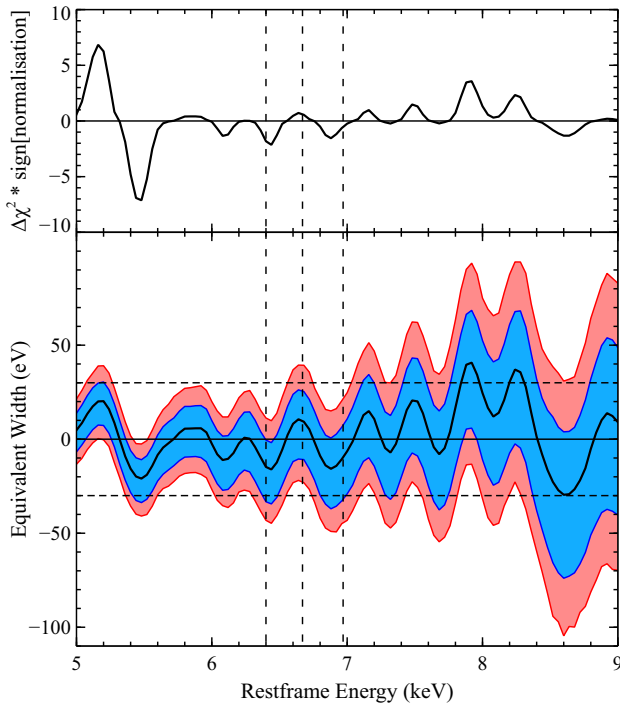


FIG. 6.— *Top panel:* the $\Delta\chi^2$ improvement obtained with the addition of a narrow Gaussian line, as a function of (rest frame) line energy, for the 2013 *XMM-Newton*+*NuSTAR* dataset. Positive (negative) values of $\Delta\chi^2$ indicate the best fit line is in emission (absorption). We find no statistically significant narrow iron K features. *Bottom panel:* 90 (blue) and 99% (red) confidence contours for the equivalent width of the narrow line, indicating the line strengths any undetected narrow features could yet have. For clarity, the rest frame transitions of neutral, helium-like and hydrogen-like iron (6.4, 6.67 and 6.97 keV) are shown with vertical dashed lines. We also plot dashed horizontal lines representing $EW = \pm 30$ eV, roughly indicative of the absorption lines seen in the Galactic BHB GRS 1915+105 (Neilsen & Lee 2009), for comparison.

the inclusion of the Gaussian line, as well as the best fit equivalent width (EW) and its 90 and 99% confidence limits, calculated with the EQWIDTH command in XSPEC, using 10,000 parameter simulations based on the best fit model parameters and their uncertainties.

The results obtained are shown in Fig. 6; the top panel shows the $\Delta\chi^2$ improvement, and the limits on EW obtained are shown in the bottom panel. For clarity, we highlight the energies of the $K\alpha$ transitions of neutral, helium-like and hydrogen-like iron, as well as $EW = \pm 30$ eV, representative of the strongest iron absorption observed in GRS 1915+105 (Neilsen & Lee 2009). As with our analysis of both Holmberg IX X-1 and NGC 1313 X-1, we find no statistically significant line detections. Any narrow atomic features in the 2013 data in the immediate Fe K band (6–7 keV) must have equivalent widths less than ~ 50 eV at 99% confidence. The line limits obtained here for Circinus ULX5 are not as stringent as those obtained most recently for Holmberg IX X-1 (Walton et al. 2013a), but are similar to those obtained previously for NGC 1313 X-1 (Walton et al. 2012a).

3.2. *Suzaku* in 2006

As with the more recent 2013 observations, the *Suzaku* spectrum obtained in 2006 is not well modelled by a simple absorbed powerlaw ($\chi^2_\nu = 1029/618$), requiring an intrinsically curved continuum instead. This is apparent from Fig. 7, in which the spectra from the three main epochs analysed (2001, 2006, 2013) are directly compared, after having

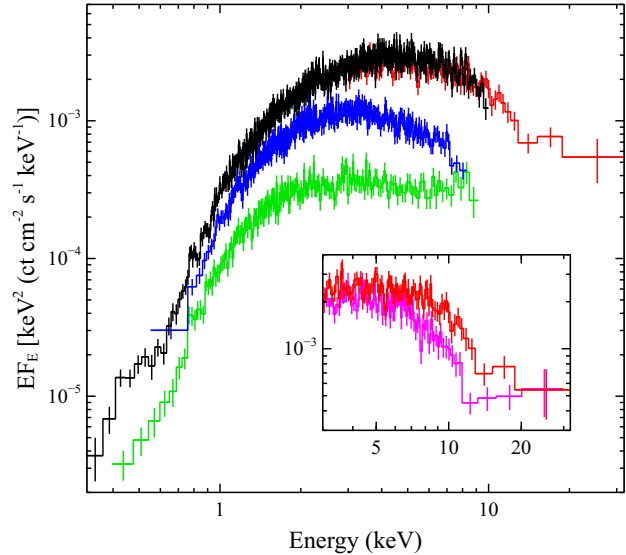


FIG. 7.— The spectral evolution displayed by Circinus ULX5. The 2013 *XMM-Newton* (EPIC-pn) and *NuSTAR* (FPMA) data are shown in black and red respectively, while the 2006 *Suzaku* (FI XIS) and the 2001 *XMM-Newton* data are shown in blue and green. The additional *NuSTAR* data are also shown in the inset in magenta, compared to the same *NuSTAR* dataset shown in the main figure. All the data have been unfolded through the same model, which simply consists of a constant.

been unfolded through the same simple model, consisting of just a constant. Indeed, the *Suzaku* data have a distinctly thermal-like appearance. However, while a DISKBB continuum gives a marked improvement and formally provides a statistically acceptable fit to the data ($\chi^2_\nu = 639/618$), an excess at high energies is again visible, broadly similar to *XMM-Newton*+*NuSTAR* dataset considered previously, albeit apparently weaker and by necessity occurring at lower energies, owing to the limited bandpass of the XIS data.

In this case, the high energy excess can be resolved by allowing for a shallower radial temperature profile for the disc with DISKPBB ($p = 0.61 \pm 0.03$), and an excellent fit is obtained ($\chi^2_\nu = 606/617$). However, this may be a consequence of the limited bandpass, so we also consider a Comptonisation origin for the high energy excess, again utilising the DISKBB+SIMPL combination. Unsurprisingly an excellent fit is also obtained with this model ($\chi^2_\nu = 590/616$; see Fig. 8), but owing to the weak excess and the lack of high energy data the SIMPL parameters are again highly degenerate, and therefore only poorly constrained individually. The observed 0.5–10.0 keV flux during this epoch, $(2.90 \pm 0.04) \times 10^{-12}$ erg cm $^{-2}$ s $^{-1}$, is significantly lower than observed in early 2013. Given the quality of fit obtained, the parameter degeneracy already present with this combination, and the lack of any obvious residuals, we do not consider the more complex DISKPBB+SIMPL, DISKBB+COMPTT or COMPTT+COMPTT models here.

3.3. *XMM-Newton* in 2001

Again, for the early (2001) *XMM-Newton* observation, we begin by modelling the data with a simple absorbed powerlaw model. Remarkably, in contrast to the two datasets considered so far, such a simple model actually provides an excellent fit to this dataset ($\chi^2_\nu = 587/580$). Again, the results obtained for the spectral parameters are presented in Table 2. In contrast, the simple accretion disk model provides a very poor fit ($\chi^2_\nu = 820/580$), with the model severely underpredicting the data

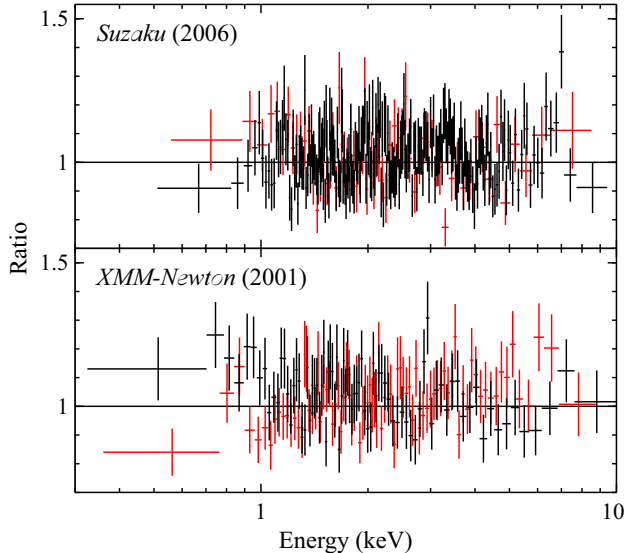


FIG. 8.— Data/model ratios for the DISKBB+SIMPL model applied to the 2006 *Suzaku* observation (*top panel*) and the 2001 *XMM-Newton* observation (*bottom panel*). Excellent fits are obtained in both cases (see Table 2). Front-illuminated XIS (*EPIC-pn*) and back-illuminated XIS (*EPIC-MOS*) data are shown in black and red respectively; the data have been rebinned for visual clarity.

above ~ 5 keV. This indicates there is a marked difference between this *XMM-Newton* observation and the later *Suzaku* and *XMM-Newton+NuSTAR* datasets, in which the spectrum below 10 keV is generally well modelled with thermal emission. The difference can clearly be seen in Fig. 7. While the *Suzaku* and *XMM-Newton+NuSTAR* datasets display curvature in the 3–10 keV bandpass, the 2001 *XMM-Newton* dataset does not, indeed appearing more consistent with an absorbed simple powerlaw-like continuum. The observed 0.3–10.0 keV flux in this observation is $(1.93 \pm 0.04) \times 10^{-12}$ erg s $^{-1}$, slightly lower again than the *Suzaku* dataset, and significantly lower than the *XMM-Newton+NuSTAR* dataset.

For completeness, we apply some of the other models considered previously as well. Statistically, the DISKBB model offers a substantial improvement on the simpler DISKBB model, however the parameters are pushed to truly extreme values ($T_{\text{in}} \simeq 5.0$ keV, $p < 0.5$) owing to the lack of curvature in the 3–10 keV bandpass. Given the flux of this observation, such an evolution of the disk would appear unphysical when compared to the more moderate parameters obtained with the other datasets. We also again consider the DISKBB+SIMPL combination, in order to investigate the results obtained interpreting the high energy ($\gtrsim 5$ keV) excess observed with the DISKBB model alone as Comptonisation. As shown in Fig. 8, this model gives an excellent fit ($\chi^2_{\nu} = 569/578$), and actually provides a reasonable improvement over the pure powerlaw continuum ($\Delta\chi^2 = 18$ for 2 additional free parameters). However, the model is again dominated by the powerlaw tail provided by the SIMPL component, and we obtain a fully consistent photon index to the pure powerlaw continuum. As with the *Suzaku* observation, given the quality of fit obtained with the DISKBB+SIMPL model, and the lack of any obvious residuals, we do not consider the more complex DISKBB+SIMPL, DISKBB+COMPTT or COMPTT+COMPTT models for this dataset, and conclude that it is best represented with a continuum dominated by a powerlaw-like component with $\Gamma \sim 2$, perhaps with some mild disc contribution at lower energies.

TABLE 3
OBSERVED 0.5–10.0 keV FRACTIONAL EXCESS VARIABILITY AMPLITUDES.

Mission	OBSID	0.5–10.0 keV F_{var} (%)
<i>XMM-Newton</i>	0111240101	15 ± 1
<i>Suzaku</i>	701036010	12 ± 1
<i>XMM-Newton</i>	0701981001	< 2

4. SHORT TERM VARIABILITY

Figure 9 shows the 0.5–10.0 keV lightcurves for the three longest duration observations, as well as the evolution of the 3–10/0.5–3.0 keV hardness ratio during these observations. Contrasting short term behaviour can be seen from each of the three observations. The long *XMM-Newton* observation in 2001 shows clear flux variability, with no strong associated spectral variability. The 2006 *Suzaku* observation also shows strong variability, although in this instance there is clear spectral variability. Indeed, this spectral variability appears to correlate extremely well with the source flux, as shown in Fig. 10, with the source displaying harder spectra at higher fluxes (note that Circinus ULX5 is vastly below the pile-up limit for *Suzaku*). Finally, in 2013, Circinus ULX5 does not appear to show any strong short term flux or spectral variability at all, although we note that of the three observations considered this has the shortest duration. In order to quantify the differing levels of variability observed, we compute the fractional excess variance (F_{var} ; Edelson et al. 2002; Vaughan et al. 2003) over the 0.5–10.0 keV energy range for each of the long observations. For consistency, we divide the earlier *XMM-Newton* and *Suzaku* observations into 2 and 3 segments of ~ 45 –50 ks duration respectively, roughly that of the latest *XMM-Newton* observation, and present the average value of F_{var} obtained from these, in order to ensure we are comparing the same timescales for each dataset. The values obtained are presented in Table 3, and confirm our earlier visual conclusions.

4.1. Spectral Variability

For the *Suzaku* observation, we also briefly investigate the nature of the observed spectral variability. First, we simply calculate the F_{var} as a function of energy. The resulting variability spectrum is shown in Fig. 11. It is clear that the fractional variability increases monotonically with increasing energy, and is strongest above the peak of the disk emission, at the energies at which the powerlaw-like tail is most prominent in the DISKBB+SIMPL model. Second, we split the observation into seven segments, ~ 15 –20 ks in duration, and spectra are extracted for each following the data reduction procedure outlined above (section 2.2.2). These seven segments are modelled simultaneously with the DISKBB+SIMPL combination, in order to investigate the behaviour of the thermal component. As the SIMPL parameters were not well constrained when considering the full time averaged spectrum, we link the photon index between all the epochs in order to minimise the effects any parameter degeneracies might have on the disk parameters obtained, which we are primarily interested in. We also link the column densities of the intrinsic absorption between the segments, as there is no strong evidence that this varies here (see also Miller et al. 2013).

With this procedure, we obtain an excellent global fit to the seven segments, with $\chi^2_{\nu} = 695/719$. In addition to the disk

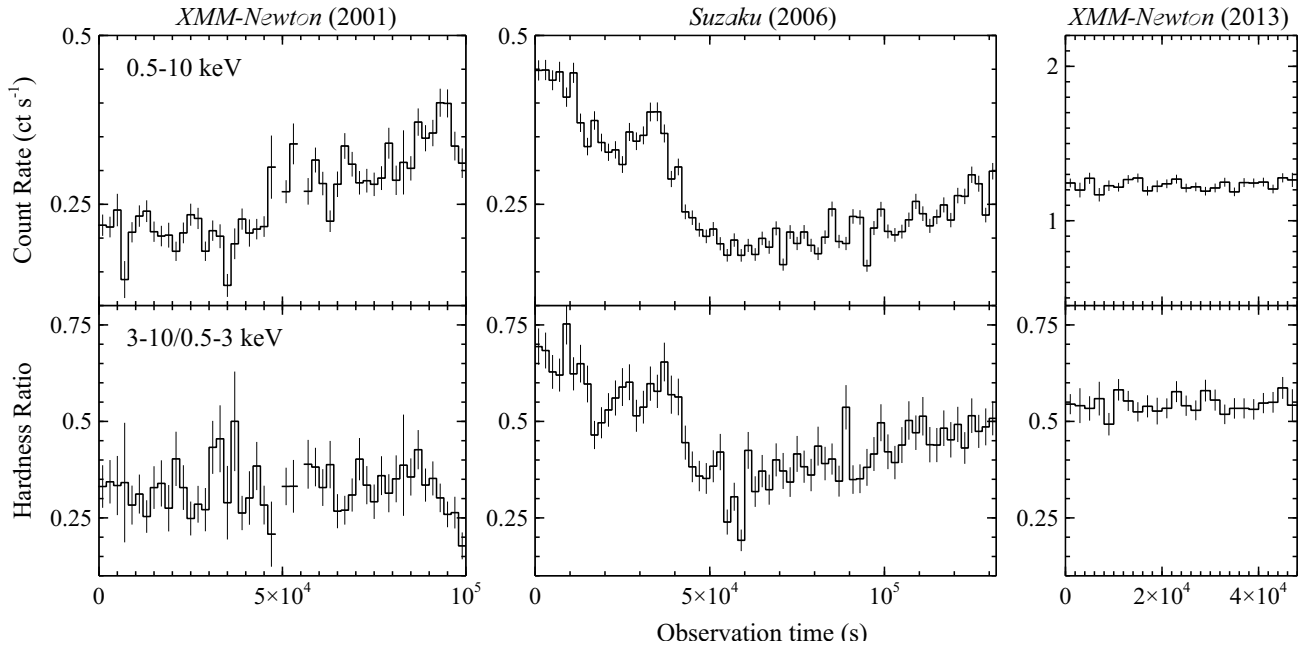


FIG. 9.— 0.5–10.0 keV lightcurves (top panels) and 3–10/0.5–3.0 keV hardness ratios (bottom panels) for the 2001 *XMM-Newton* (left panels), 2006 *Suzaku* (centre panels) and the 2013 *XMM-Newton* observations (right panels). The axes in the top panels have been scaled to show a similar dynamic range around the mean count rate for each observation. Clearly contrasting short term behaviour is seen in each of these three observations (see text).

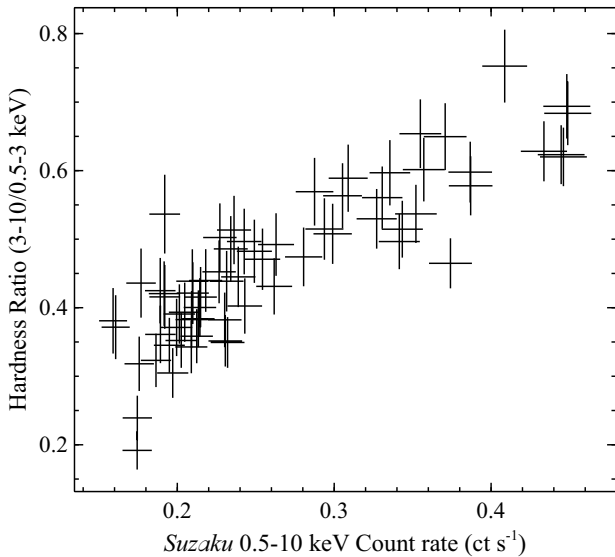


FIG. 10.— Hardness ratio–intensity diagram for the 2006 *Suzaku* observation. During this epoch, the 3–10/0.5–3.0 keV hardness ratio clearly correlates with the full 0.5–10.0 keV count rate.

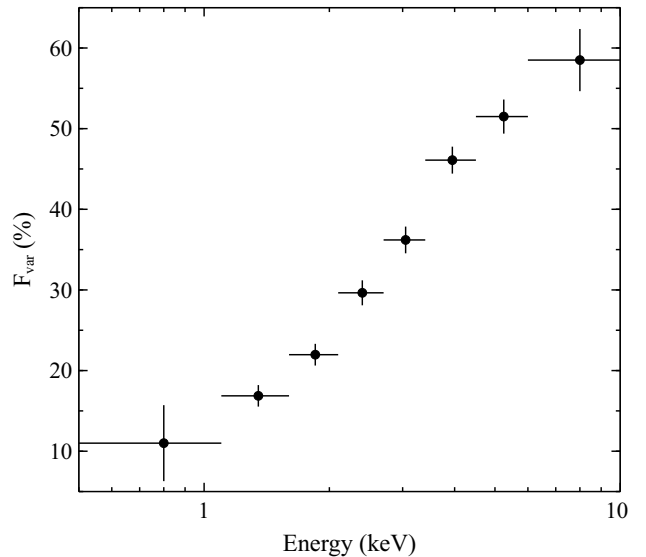


FIG. 11.— The fractional excess variance (F_{var}) as a function of energy for the 2006 *Suzaku* observation. F_{var} clearly increases with increasing energy.

temperature, which is a direct product of the model, we also compute the intrinsic disk flux for each segment with CFLUX in XSPEC. As shown in Fig. 12, there is a clear, positive correlation between the inferred flux and the temperature of the disk component. This evolution may also contribute to the energy dependence of the fractional variability. However, when modelled with a powerlaw relation, *i.e.* $L \propto T_{\text{in}}^{\alpha}$, accounting for the uncertainties on both the temperatures and the fluxes with the algorithm described in Williams et al. (2010), the exponent obtained is much shallower than the expected $L \propto T^4$ relation for a standard thin accretion disc with a constant emitting area and a constant color correction factor: $\alpha = 1.74 \pm 0.34$ (1σ uncertainty).

5. LONG TERM EVOLUTION

Given the observed correlation between the luminosity and temperature of the disk component based on the short term variability during the 2006 *Suzaku* observation, we now wish to test whether this correlation also holds for the long-term spectral evolution observed. Therefore, we take the same approach outlined previously (section 4.1) in order to investigate the evolution of the disk parameters, but here making use of multi-epoch data. In addition to the higher S/N datasets analysed previously, we also now consider the two other pointed *NuSTAR* observations, obtained either side of the observation coordinated with *XMM-Newton* (OBSIDs 30002038002 and 30002038006). The spectra from these two observations show some spectral and flux evolution when compared to the

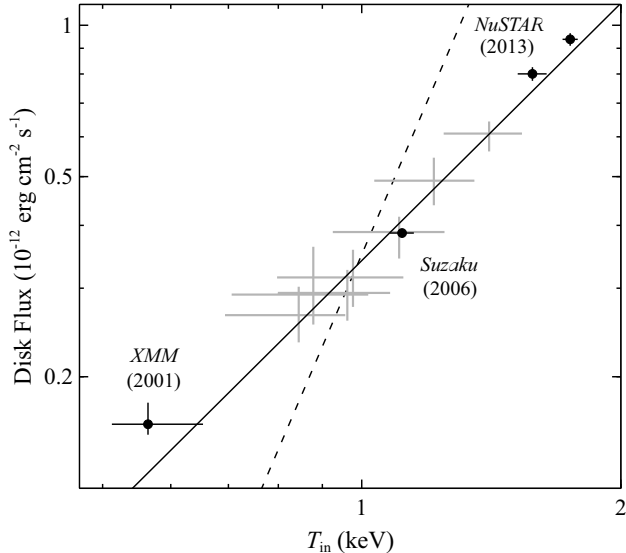


FIG. 12.— The luminosity–temperature relation inferred for the accretion disk of Circinus ULX5 when using the DISKBB+SIMPL model. The multi-epoch data are shown in black (see section 5), while the individual *Suzaku* segments considered are shown in grey (see section 4.1). Remarkably, despite probing very different timescales, all the data appear to follow a common relation, which is significantly shallower than the naively expected $L \propto T^4$ relation (shown as a dashed line) for standard stable disk emission. The solid line shows the best fit to the multi-epoch data.

NuSTAR data presented previously (see inset in Fig. 7), but are broadly consistent with one-another, and so we combine them into a single dataset for the purposes of this analysis.

This approach also provides an excellent global fit to the average spectrum from each epoch considered, with $\chi^2_\nu = 2486/2484$. The common column density obtained from all the datasets is $N_{\text{H,int}} = 1.9^{+0.2}_{-0.1} \times 10^{21} \text{ cm}^{-2}$, and the common photon index obtained is $\Gamma = 2.3^{+0.1}_{-0.2}$. Remarkably, as is clear from Fig. 12, we find that despite the observations being taken over a span of more than a decade, the multi-epoch evolution of the disk component is fully consistent with an extrapolation of the short-term evolution observed from the *Suzaku* data alone. Modeling the data again with a powerlaw relation, the multi-epoch exponent obtained is $\alpha = 1.70 \pm 0.17$, fully consistent with that obtained previously.

5.1. Flux Evolution

In addition to our analysis of the higher quality datasets available for Circinus ULX5, we also present a brief analysis of the lower S/N observations (the *Swift* snapshots, the short *Chandra* observations and the initial *NuSTAR* detection) in order to build up a long term lightcurve. Given the spectral evolution apparent in Fig. 7, we model each of these datasets with a phenomenological powerlaw continuum with a variable high-energy exponential cutoff, in order to allow for either curved or powerlaw-like continua, as favoured by each individual dataset. The neutral absorption is treated in the same manner as our more detailed spectral analysis, including both a Galactic and an intrinsic absorption component. Given the moderate quality (and/or the high energy nature) of the data, the intrinsic column is fixed at $N_{\text{H,int}} = 2.5 \times 10^{21} \text{ atom cm}^{-2}$, broadly consistent with the results obtained from the higher-quality datasets. In the case of the *Swift* observations, spectral fitting is performed through minimisation of the Cash statistic (Cash 1979) owing to the much less stringent rebinning applied to these data (see sec-

tion 2.2.4).

With this simple model, we compute the observed flux for these additional exposures in the energy band common to all the missions utilised in this work, 3–10 keV. The fluxes obtained are quoted in Table 1, and the long term lightcurve is shown in Fig. 13. Although the lightcurve is sparsely sampled given the overall span of over a decade, strong long-term variability is clearly apparent, with the 3–10 keV flux varying by at least a factor of ~ 5 , and there are two clear periods of high flux observed in early 2009 (*Chandra* datasets) and early 2013 (*NuSTAR* datasets). A more comprehensive monitoring campaign on this source would be highly beneficial, and would allow us to assess how frequently such high flux states occur.

6. DISCUSSION

6.1. Association With Circinus

Throughout this work, we have assumed that Circinus ULX5 is associated with the Circinus galaxy. Here, we present a brief discussion of whether this is likely to be the case, or whether Circinus ULX5 could plausibly be explained as distant background active galaxy, or, particularly given the low Galactic latitude of Circinus, as a foreground Galactic source.

First, we stress that the broadband X-ray spectrum of Circinus ULX5 obtained in 2013 is not consistent with that of a background AGN, which typically display powerlaw spectra (*e.g.* Piconcelli et al. 2003). Unfortunately, at the time of writing there is no Hubble coverage at the position of Circinus ULX5 with which to perform a detailed search for optical counterparts which could assist in classifying this source (*e.g.* Heida et al. 2013). Instead, we have searched for possible mid-infrared (MIR) counterparts in the wide-field *Spitzer* (Werner et al. 2004) Infrared Array Camera (IRAC; Fazio et al. 2004) map of the Circinus galaxy obtained by For et al. (2012). Fig. 14 shows MIR images of Circinus, with a wide-area $8\mu\text{m}$ view to highlight that Circinus ULX5 resides near one of the spiral arms of this galaxy, and a $4.5\mu\text{m}$ zoom-in of the X-ray position with a $4''$ radius circle illustrative of a conservative estimate for the position uncertainty. There is one MIR source within this circle, and an additional three MIR sources in close vicinity. All four sources are well detected in channel 1 ($3.6\mu\text{m}$) and channel 2 ($4.5\mu\text{m}$) of IRAC, and have relatively blue colors across this bandpass. In the Vega system, $[3.6] - [4.5] \approx 0$ for all four sources, consistent with Galactic stars and inconsistent with background AGN which typically have red MIR colors (*e.g.* Stern et al. 2005). Therefore, we do not consider it likely that Circinus ULX5 is a distant AGN being mis-identified as a ULX. Greater positional accuracy through a dedicated on-axis *Chandra* observation will be required to determine which, if any, of the *Spitzer* sources is the true NIR counterpart to Circinus ULX5, and to aid in future searches for optical counterparts.

The obvious candidates for Galactic sources that could also masquerade as a bright ULX are foreground X-ray binaries (XRBs). As the Circinus galaxy is roughly in the direction of the Galactic centre, the extent of the Galactic plane towards Circinus ULX5 is $\sim 20 \text{ kpc}$ given our own location within the Galaxy (Sale et al. 2010). Jonker & Nelemans (2004) find that the typical scale-height of XRBs out of the Galactic plane is roughly less than 1 kpc, which contributes a negligible amount to the maximum distance Circinus ULX5 could be at if within our Galaxy. Even at the highest observed

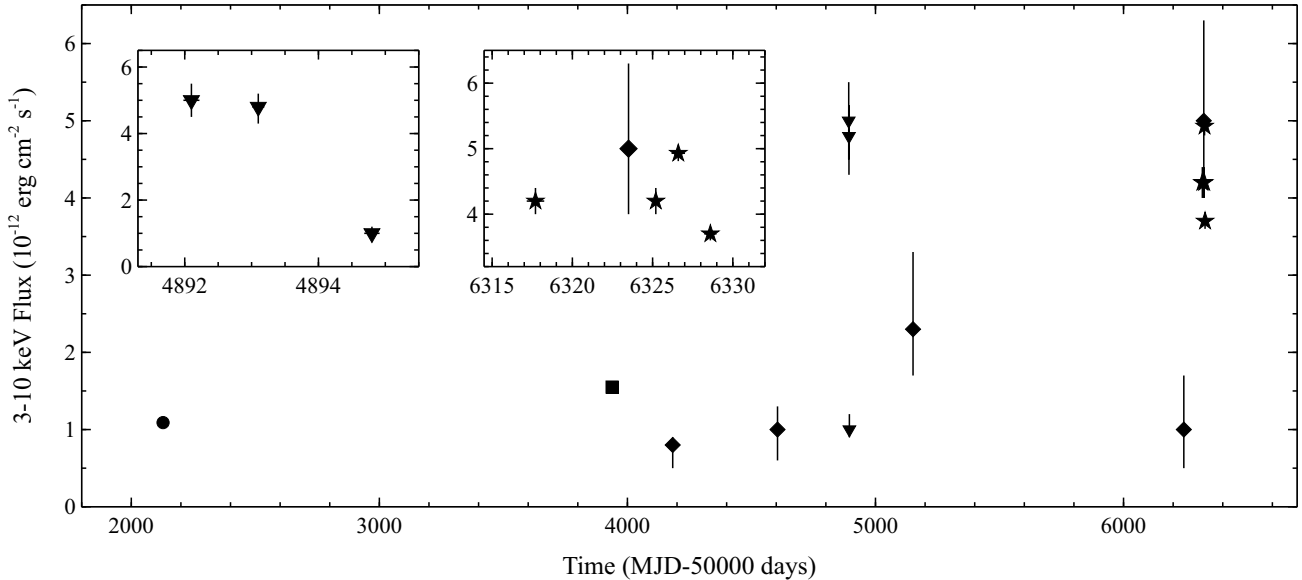


FIG. 13.— The long-term lightcurve for Circinus ULX5, covering a period of over 10 years, compiled from the new and archival data available. Periods with fairly high observing cadence are shown in insets. Fluxes obtained with *XMM-Newton*, *Suzaku*, *NuSTAR*, *Chandra* and *Swift* are indicated with circles, squares, stars, triangles and diamonds respectively.

flux in 2013, Circinus ULX5 would therefore have a luminosity of $L_X \lesssim 3 \times 10^{35} \text{ erg s}^{-1}$ if Galactic, equivalent to $L_X/L_E \lesssim 10^{-4}$ for a $10 M_\odot$ black hole. Furthermore, these observations revealed the source to have a very soft broadband spectrum. Although Galactic black hole binaries (BHs) are known to display soft spectra, these are observed at high luminosities ($L_X/L_E \gtrsim 0.1$). In contrast, low luminosity Galactic BHs are generally observed to have hard spectra (e.g. Remillard & McClintock 2006). Galactic neutron star XRBs can also display soft broadband spectra, similar to that observed, but as with Galactic BHs these are observed at high luminosities ($L_X \gtrsim 5 \times 10^{36} \text{ erg s}^{-1}$; Barret 2001).

Finally, a Galactic cataclysmic variable (CV) would be consistent with the low luminosity required to place the source in our own Galaxy. However, the observed spectrum does not appear to be consistent with those of known CVs. The high energy X-ray emission from CVs is generally observed to arise from a multi-temperature collisionally ionised plasma, either from the boundary layer between the accretion disc and the white dwarf surface for non-magnetic CVs, or from the post-shock plasma in the accretion columns for magnetic CVs; see Mukai (2005) and Kuulkers et al. (2006) for a recent reviews. However, as shown in section 3.1.3, the iron emission expected from such a plasma, which is reliably observed in known CVs (see Middleton et al. 2012 for a particularly extreme case), is not observed from Circinus ULX5. Indeed, fits to the high energy spectrum with thermal plasma models (e.g. Raymond & Smith 1977) with solar abundances fail completely. Furthermore, the spectral evolution shown in Fig. 7 is not typical behaviour for a Galactic CV.

Therefore, we conclude that none of these classes of Galactic X-ray source offers an obvious observationally self-consistent scenario for Circinus ULX5. A further point worth highlighting, throughout all our spectral modelling we always require an absorption column in excess of the Galactic column (as given in Kalberla et al. 2005), both when considering the local average for the column, and the measurement closest to the source position, which also argues against a Galactic origin for Circinus ULX5. In combination with the arguments

against a distant AGN origin presented above, this strongly supports its association with Circinus. Finally, we note that the observed variability rules out a young supernova remnant scenario for Circinus ULX5, leaving an extreme ULX (peak luminosity of $L_X \sim 2 \times 10^{40} \text{ erg s}^{-1}$) as the only plausible interpretation. In addition, as discussed in the following sections, Circinus ULX5 does display numerous similarities with other ULXs that radiate at $L_X \geq 10^{40} \text{ erg s}^{-1}$, further supporting this conclusion.

6.2. Extreme Ultraluminous X-ray Sources

Extreme ULXs with $L_X \geq 10^{40} \text{ erg s}^{-1}$ are rare, with only a few 10s identified (Walton et al. 2011b; Swartz et al. 2004, 2011). Furthermore, many of these sources are reasonably distant ($D > 10 \text{ Mpc}$; Walton et al. 2011b); extreme ULXs close enough to enable detailed study are rarer still. In this work, we have presented a multi-epoch spectral and temporal analysis of one of the few such ULXs known, Circinus ULX5, which to date has received very little observational attention, appearing only in the catalogue of Winter et al. (2006). This is likely in part due to its location with respect to the Circinus galaxy, sitting outside the D25 isophote in the relative outskirts of the galaxy, where the chances of an observed source being foreground/background are fairly high. However, as outlined previously, the association of this source with the Circinus galaxy appears to be robust.

Observationally, Circinus ULX5 appears to show a number of similarities with other extreme ULXs. First of all, the high quality datasets available when the source was fairly bright show clear curvature in the 3–10 keV bandpass (see Fig. 2). Such curvature is frequently observed in the spectra of other bright ULXs (e.g. Stobbart et al. 2006; Gladstone et al. 2009; Walton et al. 2011a, 2013a; Bachetti et al. 2013, *submitted*), and does not seem to be consistent with the powerlaw-like emission expected from a standard, optically thin sub-Eddington corona.

In addition, based on the compilation of serendipitous detections available, it is clear that Circinus ULX5 can vary in flux from epoch to epoch by at least a factor of ~ 5 (see Fig. 13 and Table 1). This, too, is broadly similar to the level of

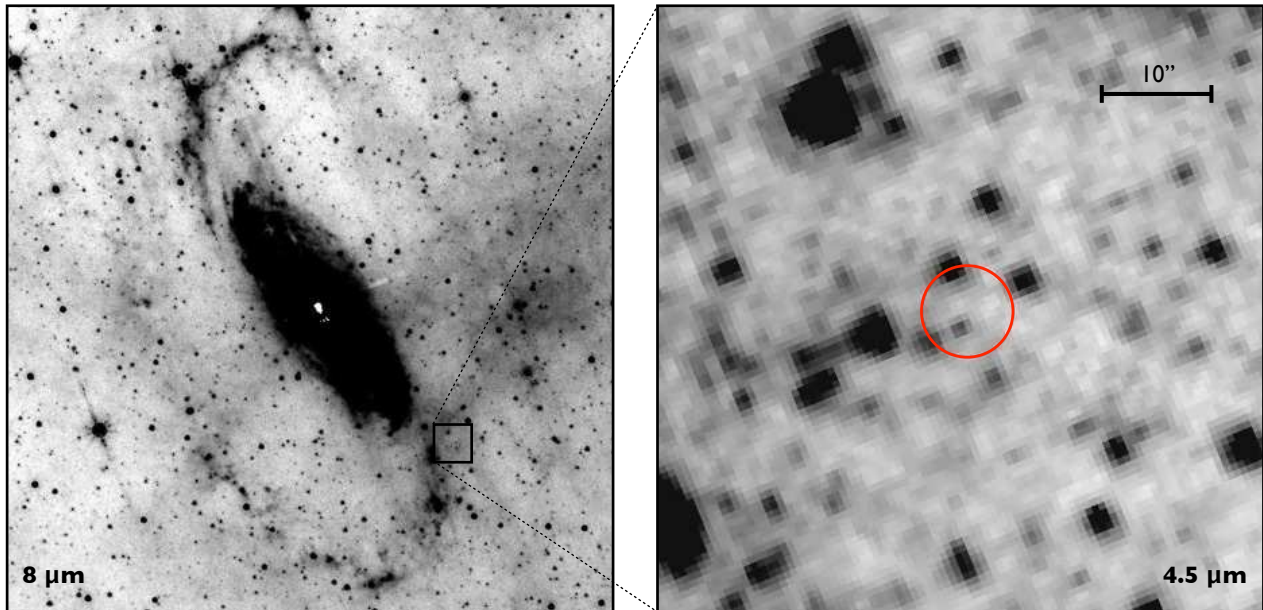


FIG. 14.— *Spitzer*/IRAC imaging of Circinus ULX5. *Left panel*: wide-field IRAC $8\ \mu\text{m}$ (channel 4) image of Circinus, 14 arcmin on a side with North up and East to the left, illustrating the location of ULX5 with respect to the spiral arms of the galaxy. *Right panel*: Close-up IRAC $4.5\ \mu\text{m}$ (channel 2), approximately 50 arcsec on a side, centered on ULX5. The red circle, with radius 4 arcsec, is centered on the *NuSTAR* position of ULX5 (RA = $14^{\text{h}}\ 12^{\text{m}}\ 39^{\text{s}}$, DEC = $-65^{\circ}\ 23'\ 34''$).

long-term variability displayed by other ULXs. For example, the recent *Swift* monitoring campaigns on Holmberg IX X-1 and NGC 5907 ULX1 revealed long term variability by a factor of ~ 3 –4 (Kong et al. 2010; Sutton et al. 2013), and multi-epoch *XMM-Newton* observations of NGC 1313 X-1 reveal long term variability by a similar factor of ~ 3 (Feng & Kaaret 2006). One potentially subtle difference is that many of the brighter ULXs appear to show suppressed short-term variability within single observations (*i.e.* timescales less than ~ 100 ks; Heil et al. 2009). In this case, we were fortunate enough to observe such variability from Circinus ULX5, particularly during the 2006 *Suzaku* observation. However, it is noteworthy that during the most recent observation of reasonable duration, when Circinus ULX5 was at its brightest, the short-term variability also appeared to be suppressed, similar to the results presented by Heil et al. (2009). Furthermore, high quality observations of ULXs with which variability can properly be studied are relatively rare, so in many cases the multi-epoch evolution of the short-term variability is not well constrained, and may well be similar to that observed here.

6.3. The Broadband X-ray Spectrum of Circinus ULX5

The *NuSTAR* observations of Circinus ULX5, along with the observations of NGC 1313 X-1, IC 342 X-1 and Holmberg IX X-1 (see Bachetti et al., *submitted*, Rana et al. and Walton et al., *in prep*, respectively), represent one of the first times it has been possible to reliably constrain the spectrum of an extreme ULX above 10 keV. In combination with *XMM-Newton*, we have been able to constrain the broadband spectral form of Circinus ULX5 over the 0.3–30.0 keV bandpass during a historically high flux state. During this epoch, Circinus ULX5 displayed numerous observational similarities at lower energies (≤ 10 keV) to previous observations of other extreme ULXs, as outlined above.

The key spectral similarity is the curvature observed in the continuum over the 3–10 keV energy range. Based on the available data, until recently limited to below 10 keV, a variety of interpretations for this curvature have been proposed

in the literature, including a high temperature accretion disk (Watarai et al. 2001), optically thick Comptonisation in a cool corona (Gladstone et al. 2009), and relativistic disk reflection (Caballero-García & Fabian 2010). The former two predict that the curvature should continue to higher energies, falling off with a thermal Wien tail, while the latter predicts a much stronger high energy spectrum owing to the Compton reflection hump (see Walton et al. 2011a).

Broadly similar to the other ULXs observed by *NuSTAR* to date, the emission above 10 keV from Circinus ULX5 is fairly weak compared to the emission below 10 keV during this epoch. The spectrum peaks at ~ 4 –5 keV, and then falls away fairly steeply. However, when the broadband *XMM-Newton*+*NuSTAR* spectrum of Circinus ULX5 is fitted with any purely thermal model with a Wien spectrum at high energies, the *NuSTAR* data shows a clear excess over the model at high energies (see Fig. 3); pure thermal models can therefore be rejected in this case. Nevertheless, the excess is not strong enough to be explained as the Compton hump if the 3–10 keV curvature is due to relativistic iron features from the inner accretion disk, so disk reflection does not appear to offer a viable solution in this case either. Instead, this high energy excess is well modelled simply as a powerlaw tail to the lower energy curved spectrum. In physical terms, the broadband spectrum can be well explained as a relatively hot accretion disk with an additional high energy Comptonised tail, or as a Comptonised spectrum from an optically thick corona of electrons with a dual temperature distribution. However, given the more straightforward comparison with the established disk-corona Galactic BHB paradigm, and the multi-epoch spectral and variability properties observed, we prefer the former.

6.4. An Emerging/Re-Emerging Accretion Disk Scenario

One of the most striking aspects of the available data for Circinus ULX5 is the clear spectral variability (see Fig. 7). During the 2001 *XMM-Newton* observation, the source appears to display a powerlaw spectrum, with no apparent curvature across the 3–10 keV energy range, while in the

higher luminosity observations obtained with *Suzaku* in 2006 and *XMM-Newton+NuSTAR* in 2013 the spectrum seems to be dominated by a thermal component, displaying the curvature across the 3–10 keV bandpass now typically associated with bright ULXs. This rather dramatic spectral evolution is reminiscent of the sub-Eddington state transitions observed in Galactic BHBs (*e.g.* Remillard & McClintock 2006; Done et al. 2007; Fender & Belloni 2012 for reviews). In particular, the evolution from the 2001 *XMM-Newton* data to the later thermal-like observations (2006, 2013) seems to be comparable to the transition from the hard/hard-intermediate state, in which the spectrum is largely dominated by the Comptonised emission from the corona, to the soft state, in which the spectrum is dominated by the thermal emission from the accretion disk.

Observation of spectral state transitions in ULXs have been claimed for a number of individual sources in the literature (*e.g.* Feng & Kaaret 2006). However, in many of these cases, the claims relate to relatively subtle changes in the observed spectrum, rather than true evidence for state transitions in the traditional sense displayed by Galactic BHBs, particularly when one bears in mind that the same state can be observed in the same source over a range of luminosities. Nonetheless, there are some ULXs that show spectral evolution as strong as observed in Circinus ULX5. The most compelling case for sub-Eddington transitions is also the most luminous ULX currently known, ESO 243-49 HLX-1 (Farrell et al. 2009), with strong spectral evolution that follows the characteristic state-transition cycle displayed by Galactic BHBs in outburst (Servillat et al. 2011). However, in many respects ESO 243-49 HLX-1 is rather unique, displaying apparently periodic outburst cycles over which the flux varies by more than an order of magnitude (Lasota et al. 2011; Godet et al. 2012), and the peak luminosity ($L_X \sim 10^{42}$ erg s $^{-1}$) is vastly in excess of that reached by the majority of ULXs, so we caution against drawing strong comparisons between ESO 243-49 HLX-1 and the rest of the ULX population, including Circinus ULX5. However, amongst the more ‘standard’ ULX population there have been a few cases in which the spectral evolution appears similar to that presented here, notably for the ULXs in IC 342 (Kubota et al. 2001b, 2002).

Indeed, although we have also considered more complex models, the high quality spectra available from multiple epochs are all well modelled with a simple combination of an accretion disk and a high energy Comptonised tail. As the source becomes more luminous, the accretion disk becomes more prominent with this combination, broadly similar to the behaviour observed from Galactic BHBs. This is emphasized in Fig. 15, which shows both the total model and the relative DISKBB contribution for the 2013 *XMM-Newton+NuSTAR* and the 2001 *XMM-Newton* datasets (*i.e.* the limiting flux cases) obtained with our joint analysis of all the high S/N datasets with the DISKBB+SIMPL model combination (see section 5). The variability behaviour observed from Circinus ULX5 would also appear to support this evolution, when considered in comparison to Galactic BHBs. Clear short-term variability is observed in the two lower flux observations, in which the coronal emission is most prominent. In particular, during the *Suzaku* observation, we see that the fractional variability is stronger at higher energies (see Fig. 11), where the coronal emission dominates. In contrast, during the highest flux observation, in which the disk emission dominates below 10 keV, no short-term variability is observed. In Galactic BHBs, short-term variability is also asso-

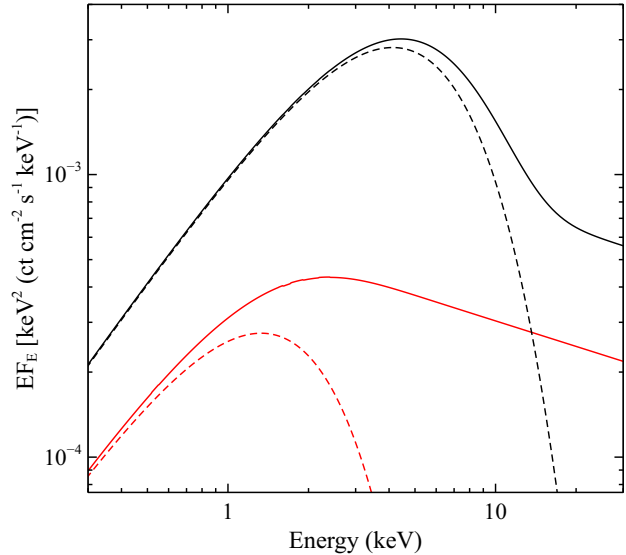


FIG. 15.— The total (unabsorbed) model (*solid lines*) and the relative contribution of the accretion disk (*dashed lines*) for the 2013 *XMM-Newton+NuSTAR* (*black*) and 2001 *XMM-Newton* (*red*) observations, obtained with our joint analysis of all the high S/N datasets with the DISKBB+SIMPL model (see section 5). The relative contribution of the accretion disk over the analysed 0.3–30 keV energy range is much greater in the high flux case.

ciated with strong coronal emission (*e.g.* Homan et al. 2001; Churazov et al. 2001), with the harder states generally displaying strong variability. In contrast, the thermal-dominated states display very little variability, with the emission dominated by a relatively stable accretion disk. The behaviour of Circinus ULX5 is strikingly similar.

However, identifying the spectral evolution in Circinus ULX5 with the hard-to-soft state transition as seen in Galactic BHBs is not necessarily straightforward. In Galactic sources, hard states (the canonical low/hard state and the hard-intermediate state) can be observed at luminosities up to roughly 10–30% of the Eddington limit (L_E). If we identify the luminosity observed in the 2001 *XMM-Newton* observation with this Eddington ratio (*i.e.* $L_X/L_E = 0.3$, to be relatively conservative), the implied black hole mass is $M_{BH} \gtrsim 90 M_\odot$. For the same spin, Eddington ratio and color correction factor, the accretion disc temperature of such a black hole should be a factor of at least ~ 1.7 cooler than for a black hole of mass $10 M_\odot$. Accretion disks observed from Galactic BHBs in the classical hard state are already rather cool, with $T_{in} \sim 0.2$ keV (*e.g.* Reis et al. 2009, 2010; Reynolds & Miller 2013). However, the disk temperatures obtained here are actually rather similar to those observed from such sub-Eddington Galactic BHBs at higher luminosities: $T_{in} \sim 0.5$ keV in the intermediate states and ~ 1 – 2 keV in the disk-dominated states (see Reynolds & Miller 2013).

Furthermore, although there is a clear positive correlation between the temperature and inferred luminosity of the disk (see Fig. 12), which remarkably seems to hold across all the timescales and luminosities currently probed, the observed relation is $L \propto T_{in}^\alpha$ with $\alpha = 1.78 \pm 0.19$, much shallower than the theoretically expected relation for a standard, geometrically stable thin disk (*i.e.* $L \propto T^4$). While Galactic BHBs do themselves frequently show significant deviations from this relation (*e.g.* Dunn et al. 2011; Reynolds & Miller 2013), the strongest deviations tend to be seen either when the coronal emission was strong (*i.e.* hard states), probably linked

to strong irradiation of the disk, or very high luminosities, at which the scale height of the disk should start to increase and advection becomes increasingly important. During the thermal-dominated state, and while the disk remains thin, the observed luminosity-temperature relation does tend to follow expectation relatively well (see also Gierliński & Done 2004). At low luminosities, the deviations away from $L \propto T^4$ tend to be in the sense that the disk temperature is less dependent on the luminosity, becoming almost constant (Reynolds & Miller 2013). In contrast, the Circinus ULX5 disk temperature displays a stronger dependence on luminosity than expected.

This is instead more similar to the behaviour observed from another ULX, NGC 1313 X-2, based on the results obtained by Kajava & Poutanen (2009) modelling *XMM-Newton* and *Chandra* data with a pure DISKBB model ($\alpha = 2.39 \pm 0.16$). It is also similar to the deviations from $L \propto T^4$ displayed by the Galactic BHBs GRO J1655–40 and XTE J1550–564 during the higher luminosity stages of their respective outbursts, when the sources were in the very-high state (Kubota et al. 2001a; Kubota & Makishima 2004; Saito et al. 2006). Sources in the very-high state also display strong Comptonised emission, but with steeper spectra and at substantially higher luminosities than the more traditional hard states (Remillard & McClintock 2006). However, it is interesting to note that, for the latter cases, these deviations are still seen at sub-Eddington luminosities. XTE J1650–500, another sub-Eddington Galactic BHB, also seems to display similar behaviour, although these data are more limited (Gierliński & Done 2004).

The observed accretion disk evolution can depart from the naively expected $L \propto T^4$ relation for a variety of reasons, which can be roughly separated into changes in the disk geometry (*i.e.* emitting area) and changes in the detailed plasma physics of the disk atmosphere (*e.g.* temperature dependent opacities, evolving vertical structure and dissipation profiles, *etc.*). The former primarily relates to changes in the inner radius, R_{in} , while the latter potentially incorporates a variety of complex effects that are difficult to isolate observationally, and so the combined effect is instead typically quantified as a multiplicative color-correction factor, that relates the effective mid-plane temperature of the disk to that actually observed: $T_{\text{in}} = f_{\text{col}} T_{\text{eff}}$. For simplicity, f_{col} is usually assumed to be energy independent, such that it only serves to shift the observed temperature of the disc, rather than modify its spectral form. A substantial body of work has been undertaken attempting to theoretically determine the expected values of f_{col} across a wide range of accretion regimes, *e.g.* Shimura & Takahara (1995); Merloni et al. (2000); Fabian et al. (2004); Davis et al. (2005), which typically suggest that $f_{\text{col}} \sim 1.7$ for disk-dominated sub-Eddington accretion. Here we are primarily interested in the relative rather than the absolute behaviour of f_{col} . The disk should evolve as $L \propto R_{\text{in}}^2 T_{\text{eff}}^4$, hence variation in either R_{in} or f_{col} can result in the relation between the luminosity and the observed temperature deviating from $L \propto T_{\text{in}}^4$. In order to recover the luminosity-temperature relation observed for Circinus ULX5, either the inner radius of the disk must decrease with increasing luminosity as $R_{\text{in}} \propto L^{-0.6}$ (for a constant f_{col}), or the color-correction factor must increase with luminosity as $f_{\text{col}} \propto L^{0.3}$ (for a constant R_{in}), or some combination of these effects is present (observationally, changes in R_{in} and f_{col} are unfortunately highly degenerate, particularly for the simple models employed here). Therefore, given the inferred range in disk luminosity, either R_{in} decreased by

up to a factor of ~ 2.9 , or f_{col} increased by up to a factor of ~ 1.7 between the 2001 and 2013 observations.

If we invoke a variable R_{in} to explain the observed spectral evolution, the implication is that the disk was truncated beyond the innermost stable circular orbit at least during the lower flux observations. Substantial truncation of the accretion disk is only really expected at very low accretion rates ($L/L_E \lesssim 10^{-2}$), in the low-luminosity regime of the hard state (*e.g.* Tomsick et al. 2009). However, while the spectrum of Circinus ULX5 during the 2001 *XMM-Newton* observation could be considered relatively hard, particularly in comparison to the more recent observations, and can be modeled simply as a powerlaw, it does not seem consistent with expectations for such a low-Eddington regime, during which Galactic BHBs typically display very hard spectra ($\Gamma \lesssim 1.7$). Instead, the photon index obtained would suggest one of the higher luminosity hard state manifestations (if the source was in this regime at all). While it could be debated whether a factor of ~ 3 change in inner radius is ‘substantial’ truncation, studies into the evolution of the relativistic iron line profiles observed from Galactic BHBs at various stages of their outbursts seem to rule out changes in the inner radius even of this magnitude as sources evolve from the higher luminosity hard states to the soft state (Reis et al. 2011; Walton et al. 2012b), and a variable f_{col} has been proposed as an alternative explanation for the continuum evolution seen at these luminosities (*e.g.* Reynolds & Miller 2013; Salvesen et al. 2013). In any case, as stated previously, the observed behaviour seems to compare far more favourably to high-luminosity observations of Galactic BHBs, where disk truncation is not expected, but evolution in the vertical structure of the disk is. Therefore, it seems likely that the deviation away from $L \propto T_{\text{in}}^4$ is driven by a variable f_{col} in this case.

The identification of Circinus ULX5 as a (reasonably) high-Eddington black hole binary system actually appears to provide a fairly self-consistent picture, at least to first order, when considered in the context of the observed/expected behaviour of Galactic BHBs. As discussed previously, the observed luminosity-temperature relation appears extremely similar to that inferred from known Galactic binaries at high luminosity, and seems to require a color-correction factor that increases with increasing luminosity. Theoretical consideration of the expected evolution of f_{col} suggest that the opposite trend should be seen at low luminosities (Merloni et al. 2000), which appears to be supported by observation (Reynolds & Miller 2013; Salvesen et al. 2013). Furthermore, the spectrum during the 2001 *XMM-Newton* observation, which shows strong Comptonised emission, is remarkably similar to that observed from both XTE J1550–564 and GRO J1655–40 at the transition (referred to by Kubota et al. as the ‘anomalous regime’) between the classic thermal state in which the sources follow $L \propto T_{\text{in}}^4$ rather well, implying a constant f_{col} , and the higher luminosities at which they appear to deviate from this relation.

This is potentially of key importance, as it could provide an anchor from which to estimate the relative luminosity of Circinus ULX5, under the assumption that this transition occurs over a fairly narrow range of L/L_E . Although this is a fairly strong assumption, as the behaviour of Galactic BHBs can be quite diverse, XTE J1550–564 and GRO J1655–40 seem to make this transition at $L/L_E \sim 0.3$ and 0.1 respectively (Gierliński & Done 2004). Conservatively adopting the former for the 2001 *XMM-Newton* observation, we return to the previous estimate of $M_{\text{BH}} \sim 90 M_{\odot}$. However, associat-

ing Circinus ULX5 with this accretion regime, rather than the canonical low/hard state, has the advantage that the *XMM-Newton* disk temperature is indeed lower than the temperatures observed from both XTEJ1550-564 and GRO J1655-40 during the relevant transition ($T_{\text{in}} \sim 1$ keV), by roughly the factor expected for a $\sim 90 M_{\odot}$ black hole compared to a $\sim 10 M_{\odot}$ black hole. However, in the absence of any dynamical information on the putative binary system, and given the diversity in the behaviour observed from Galactic BHB accretion disks (Gierliński & Done 2004; Dunn et al. 2011; Reynolds & Miller 2013), this mass estimate must still be considered speculative, and treated with the appropriate caution. Furthermore, we also urge caution in extrapolating the proposed identification of Circinus ULX5 to the general ULX population, as it is based on the specific behaviour displayed by this source.

Such a black hole is just about at the upper limit of the mass range it is currently believed possible to form *in situ* via standard stellar evolution (Zampieri & Roberts 2009; Belczynski et al. 2010). This would appear to require a low metallicity, $Z \sim 0.05 Z_{\odot}$ or less. The work by Oliva et al. (1999) does suggest the Circinus galaxy has a sub-solar metallicity, although at roughly $\sim 0.5 Z_{\odot}$ this may not be low enough to form such a black hole directly. If this mass is correct, more exotic formation mechanisms (e.g. Portegies Zwart et al. 2004) may be required. However, the metallicity estimates in Oliva et al. (1999) are based in circumnuclear clouds rather than the immediate environment around Circinus ULX5. Therefore, given that the mass is still ultimately uncertain, we defer detailed discussion of possible formation scenarios until more secure mass estimates and further studies focusing on the immediate environment of Circinus ULX5 are available.

If our identification of the accretion regime displayed by Circinus ULX5 is correct, then in the most recent high flux state we are observing the *re-emergence* of the accretion disk as it again begins to dominate over the very-high state corona, and in principle at lower luminosities the X-ray spectrum should also appear disk-dominated, as the source returns to the more traditional thermal state. Tao & Blaes (2013) suggest the very-high state corona could be related to the vertical structure of the disk at high luminosities, and are able to reproduce similar spectra to those observed with vertical dissipation profiles that dissipate more energy at larger scale heights, in the hot, ionised upper layers of the disk atmosphere. This disk state could also be described as having an *energy dependent* f_{col} , or alternatively a distribution of f_{col} values, that produces the hard tail. This is potentially physically distinct from the corona that dominates during the low/hard state, which may well be associated with the base of a jet (Markoff et al. 2005; Miller et al. 2012; Reis & Miller 2013).

In order to explain the observations of Circinus ULX5 as an extension of the high luminosity behaviour of Galactic binaries, all of which are fully driven by an evolving disk structure and without invoking very large mid-plane disk temperatures, the evolution could roughly be along the following lines. As the source increases in luminosity from the classic thermal state, the characteristic height of the dissipation profile first increases relative to the scale height of the disc, such that more energy is dissipated in the scattering atmosphere and a strong, high energy tail emerges. Increasing the luminosity further still, the scale height of the disc also increases and in effect catches up with the dissipation profile, such that more of

the energy is again dissipated in the optically-thick regions of the disk, and the blackbody-like emission progressively dominates again.

Obtaining lower flux observations may therefore provide a simple test of our proposed identification. This would most likely require dedicated monitoring in order to identify and follow up periods of low flux. Although the temperature of the disk should decrease further, the evolution should switch to roughly following $L \propto T_{\text{in}}^4$, which would alleviate the rate of decrease, keeping the disk in the band observable with current soft X-ray instrumentation for a wide range of luminosities.

6.5. Super-Eddington Accretion and X-ray Outflows

Galactic binaries in disk-dominated states frequently display evidence for outflows in the form of narrow, highly-ionised iron absorption (e.g. Miller et al. 2006; Neilsen & Lee 2009; Ponti et al. 2012; King et al. 2012). Furthermore, in agreement with basic expectation, the strength of these outflows appears to increase with increasing luminosity (Ponti et al. 2012). This prompted us to search for evidence of similar features in the joint *XMM-Newton*+*NuSTAR* dataset obtained in 2013, which offers both the best photon statistics in the iron $K\alpha$ band and the highest source luminosity of the higher quality datasets available (see section 3.1.3).

Similar to our analysis of other bright ULXs (Walton et al. 2012a, 2013a), we do not find any statistically compelling narrow iron features in either absorption or emission, so in Fig. 6 we present the equivalent width limits on any narrow lines that could have been present and remain undetected. Across the immediate Fe K bandpass (6–7 keV), any emission/absorption lines must have $EW \lesssim 50$ eV. Although these limits are not as stringent as recently obtained for Holmberg IX X-1 (Walton et al. 2013a), in absolute terms they still require any lines to be weaker than the strongest features seen in Galactic BHBs (King et al. 2012). Metallicity is likely to be an issue here, with Oliva et al. (1999) estimating the (circumnuclear) iron abundance to be $A_{\text{Fe/solar}} \sim 0.4$. However, even accounting for this iron abundance, the limits obtained still rule out the line strengths that might be expected from simple scaling of the features in e.g. GRS 1915+105 (~ 30 eV; Neilsen & Lee 2009) up to the Eddington ratio that would be inferred for a black hole of mass $\sim 10 M_{\odot}$ ($EW \gtrsim 200$ eV). Thus, it seems likely that we cannot be viewing the central regions of Circinus ULX5 through any extreme super-Eddington outflow. Similar conclusions were drawn for Holmberg IX X-1 and NGC 1313 X-1. However, as noted earlier, we again stress that the local metallicity is not well constrained, which if substantially lower than the circumnuclear metallicity would further hinder line detection. Nevertheless, a larger black hole accreting at a lower Eddington rate also offers a plausible explanation for the lack of ionised absorption, as the solid angle subtended by outflows launched from the accretion disk is widely expected to increase with increasing Eddington luminosity (e.g. King 2009; Dotan & Shaviv 2011; Kawashima et al. 2012), thus for a given observed luminosity there should be a larger range of viewing angles that do not intercept any outflow launched for larger black hole masses.

In addition, any iron emission must be weaker than observed from many Galactic high mass X-ray binaries (HMXBs). Iron emission is ubiquitously observed from such sources (Torrejón et al. 2010), as they illuminate the strong stellar winds launched by their massive binary companions. Following the discussion outlined in Walton et al. (2013a) for Holmberg IX X-1, we argue that the lack of strong iron emis-

sion suggests that any stellar wind launched by the companion of Circinus ULX5 is probably not sufficient to power the observed X-ray luminosities via wind-fed accretion, and thus Circinus ULX5 most likely accretes via Roche-lobe overflow.

7. CONCLUSIONS

Prompted by a serendipitous detection with the *NuSTAR* observatory, we have undertaken a multi-epoch spectral and temporal analysis of an extremely luminous ULX located in the outskirts of the Circinus galaxy, utilising data from most of the major X-ray observatories operating over the last decade, including coordinated follow-up observations with *XMM-Newton* and *NuSTAR*. Based on previous detections of ULX candidates in Circinus, we refer to this source Circinus ULX5. The *NuSTAR* data presented here represent one of the first instances of a ULX reliably detected at hard ($E > 10$ keV) X-rays. Circinus ULX5 is observed to vary on long timescales by at least a factor of ~ 5 , and was caught in a historically bright state by our 2013 observations, with an observed 0.3–30.0 keV luminosity of 1.6×10^{40} erg s $^{-1}$. During this epoch, the source displayed a curved 3–10 keV spectrum, broadly similar to other bright ULXs. We consider a variety of models for the broadband 0.3–30.0 keV spectrum obtained. Pure thermal models (direct accretion disk emission, cool optically thick Comptonization) result in a high energy excess in the *NuSTAR* data, and require a second emission component. However, this excess is too weak for the Compton reflection interpretation previously proposed for the 3–10 keV curvature in other ULXs.

In addition to the flux variability observed, Circinus ULX5 also displays strong spectral variability from epoch to epoch, and even at times within a single epoch. All the high quality datasets currently available are well modelled with a simple combination of thermal accretion disk emission and a Comptonized corona, an interpretation which is further supported by the observed short-term variability properties. As the source luminosity increases, the accretion disk becomes more prominent. However, although the disk temperature and luminosity follow a common relation across all timescales probed, the observed relation is much shallower than the $L \propto T^4$ relation naively expected for blackbody radiation, varying instead as $L \propto T^{1.7}$. The spectral variability displayed by Circinus ULX5 is extremely reminiscent of that observed from the Galactic BHBs XTE J1550-564 and GRO J1655-40 at high luminosities, which also seem to roughly follow $L \propto T^2$. Identifying the lowest luminosity observation of Circinus ULX5 with the transition into the $L \propto T^2$ regime, as the spectral comparison would suggest, implies a black hole mass of $\sim 90 M_{\odot}$. This is also consistent with the lower disk temperature displayed by Circinus ULX5 during this epoch. However, we stress that given the fairly diverse behaviour observed from Galactic BHB accretion disks, this mass estimate should be considered highly uncertain. Further study of this remarkable source is certainly warranted in order to see if this mass estimate truly holds up to scrutiny.

Finally, during the highest flux observation, we find no evidence for any iron features in either emission or absorption, similar again to other bright ULXs. Any features intrinsically present in the immediate Fe K bandpass must have $EW \lesssim 50$ eV. The implication is that we are not viewing the central regions of Circinus ULX5 through any extreme super-Eddington outflow, which would also be consistent with Circinus ULX5 hosting a relatively massive black hole.

ACKNOWLEDGEMENTS

The authors thank Koji Mukai for useful discussion regarding Galactic CVs, and Rubens Reis for discussion regarding Galactic BHBs. This research has made use of data obtained with the *NuSTAR* mission, a project led by the California Institute of Technology (Caltech), managed by the Jet Propulsion Laboratory (JPL) and funded by NASA, *XMM-Newton*, an ESA science mission with instruments and contributions directly funded by ESA Member States and NASA, the *Suzaku* observatory, a collaborative mission between the space agencies of Japan (JAXA) and the USA (NASA). In addition, this research has also made use of data obtained from NASAs *Swift*, *Chandra* and *Spitzer* satellites. We thank the *NuSTAR* Operations, Software and Calibration teams for support with the execution and analysis of these observations. This research has made use of the *NuSTAR* Data Analysis Software (NUSTARDAS) jointly developed by the ASI Science Data Center (ASDC, Italy) and Caltech (USA). We also made use of the NASA/IPAC Extragalactic Database (NED), which is operated by JPL, Caltech, under contract with NASA. Some of the figures included in this work have been produced with the *Veusz* plotting package: <http://home.gna.org/veusz>, written and maintained by Jeremy Sanders. FEB acknowledges support from Basal-CATA (PFB-06/2007) and CONICYT-Chile (under grants FONDECYT 1101024 and Anillo ACT1101). MB wishes to acknowledge the support from the Centre National D'Études Spatiales (CNES).

REFERENCES

- Abramowicz M. A., Czerny B., Lasota J. P., Szuszkiewicz E., 1988, *ApJ*, 332, 646
- Arnaud K. A., 1996, in *Astronomical Data Analysis Software and Systems V*, edited by G. H. Jacoby & J. Barnes, vol. 101 of *Astronomical Society of the Pacific Conference Series*, 17
- Barret D., 2001, *Advances in Space Research*, 28, 307
- Bauer F. E., Brandt W. N., Sambruna R. M., et al., 2001, *AJ*, 122, 182
- Bauer F. E., Dwarkadas V. V., Brandt W. N., et al., 2008, *ApJ*, 688, 1210
- Belczynski K., Bulik T., Fryer C. L., et al., 2010, *ApJ*, 714, 1217
- Caballero-García M. D., Fabian A. C., 2010, *MNRAS*, 402, 2559
- Cash W., 1979, *ApJ*, 228, 939
- Churazov E., Gilfanov M., Revnivtsev M., 2001, *MNRAS*, 321, 759
- Corongiu A., Chiappetti L., Haardt F., Treves A., Colpi M., Belloni T., 2003, *A&A*, 408, 347
- Dauser T., Wilms J., Reynolds C. S., Brenneman L. W., 2010, *MNRAS*, 409, 1534
- Davis S. W., Blaes O. M., Hubeny I., Turner N. J., 2005, *ApJ*, 621, 372
- Done C., Gierliński M., Kubota A., 2007, *A&A Rev.*, 15, 1
- Dotan C., Shaviv N. J., 2011, *MNRAS*, 413, 1623
- Dunn R. J. H., Fender R. P., Körding E. G., Belloni T., Merloni A., 2011, *MNRAS*, 411, 337
- Edelson R., Turner T. J., Pounds K., et al., 2002, *ApJ*, 568, 610
- Fabian A. C., Ross R. R., Miller J. M., 2004, *MNRAS*, 355, 359
- Farrell S. A., Webb N. A., Barret D., Godet O., Rodrigues J. M., 2009, *Nat.*, 460, 73
- Fazio G. G., Hora J. L., Allen L. E., et al., 2004, *ApJS*, 154, 10
- Fender R., Belloni T., 2012, *Science*, 337, 540
- Feng H., Kaaret P., 2006, *ApJ*, 650, L75
- Feng H., Soria R., 2011, *NAR*, 55, 166
- Finke J. D., Böttcher M., 2007, *ApJ*, 667, 395
- For B.-Q., Koribalski B. S., Jarrett T. H., 2012, *MNRAS*, 425, 1934
- Freeman K. C., Karlsson B., Lynga G., et al., 1977, *A&A*, 55, 445
- Garmire G. P., Bautz M. W., Ford P. G., Nousek J. A., Ricker Jr. G. R., 2003, in *SPIE Conference Series*, edited by J. E. Truemper, H. D. Tananbaum, vol. 4851 of *SPIE Conference Series*, 28–44
- Gehrels N., Chincarini G., Giommi P., et al., 2004, *ApJ*, 611, 1005

- Gierliński M., Done C., 2004, *MNRAS*, 347, 885
- Gladstone J. C., Roberts T. P., Done C., 2009, *MNRAS*, 397, 1836
- Godet O., Webb N., Barret D., Farrell S., Gerhels N., Servillat M., 2012, *The Astronomer's Telegram*, 4327, 1
- Harrison F. A., Craig W. W., Christensen F. E., et al., 2013, *ApJ*, 770, 103
- Heida M., Jonker P. G., Torres M. A. P., et al., 2013, *ArXiv e-prints*
- Heil L. M., Vaughan S., Roberts T. P., 2009, *MNRAS*, 397, 1061
- Homan J., Wijnands R., van der Klis M., et al., 2001, *ApJS*, 132, 377
- Ishida M., Tsujimoto M., Kohmura T., et al., 2011, *PASJ*, 63, 657
- Jansen F., Lumb D., Altieri B., et al., 2001, *A&A*, 365, L1
- Jonker P. G., Heida M., Torres M. A. P., et al., 2012, *ApJ*, 758, 28
- Jonker P. G., Nelemans G., 2004, *MNRAS*, 354, 355
- Kajava J. J. E., Poutanen J., 2009, *MNRAS*, 398, 1450
- Kalberla P. M. W., Burton W. B., Hartmann D., et al., 2005, *A&A*, 440, 775
- Kawashima T., Ohsuga K., Mineshige S., Yoshida T., Heinzeller D., Matsumoto R., 2012, *ApJ*, 752, 18
- King A. L., Miller J. M., Raymond J., et al., 2012, *ApJ*, 746, L20
- King A. R., 2009, *MNRAS*, 393, L41
- Kong A. K. H., Yang Y. J., Yen T.-C., Feng H., Kaaret P., 2010, *ApJ*, 722, 1816
- Koribalski B. S., Staveley-Smith L., Kilborn V. A., et al., 2004, *AJ*, 128, 16
- Koyama K., Tsunemi H., Dotani T., et al., 2007, *PASJ*, 59, 23
- Kubota A., Done C., Makishima K., 2002, *MNRAS*, 337, L11
- Kubota A., Makishima K., 2004, *ApJ*, 601, 428
- Kubota A., Makishima K., Ebisawa K., 2001a, *ApJ*, 560, L147
- Kubota A., Mizuno T., Makishima K., et al., 2001b, *ApJ*, 547, L119
- Kuulkers E., Norton A., Schwobe A., Warner B., 2006, X-rays from cataclysmic variables, 421–460
- Lasota J.-P., Alexander T., Dubus G., et al., 2011, *ApJ*, 735, 89
- Li L.-X., Zimmerman E. R., Narayan R., McClintock J. E., 2005, *ApJS*, 157, 335
- Liu Q. Z., Mirabel I. F., 2005, *A&A*, 429, 1125
- Makishima K., Takahashi H., Yamada S., et al., 2008, *PASJ*, 60, 585
- Markoff S., Nowak M. A., Wilms J., 2005, *ApJ*, 635, 1203
- Merloni A., Fabian A. C., Ross R. R., 2000, *MNRAS*, 313, 193
- Middleton M. J., Cackett E. M., Shaw C., Ramsay G., Roberts T. P., Wheatley P. J., 2012, *MNRAS*, 419, 336
- Middleton M. J., Miller-Jones J. C. A., Markoff S., et al., 2013, *Nat*, 493, 187
- Middleton M. J., Sutton A. D., Roberts T. P., 2011, *MNRAS*, 417, 464
- Miller J. M., Fabbiano G., Miller M. C., Fabian A. C., 2003, *ApJ*, 585, L37
- Miller J. M., Pooley G. G., Fabian A. C., et al., 2012, *ApJ*, 757, 11
- Miller J. M., Raymond J., Fabian A. C., et al., 2006, *Nat*, 441, 953
- Miller J. M., Raymond J., Fabian A. C., et al., 2004, *ApJ*, 601, 450
- Miller J. M., Walton D. J., King A. L., et al., 2013, *ArXiv e-prints*
- Mineshige S., Hirano A., Kitamoto S., Yamada T. T., Fukue J., 1994, *ApJ*, 426, 308
- Mitsuda K., Bautz M., Inoue H., et al., 2007, *PASJ*, 59, 1
- Mitsuda K., Inoue H., Koyama K., et al., 1984, *PASJ*, 36, 741
- Mukai K., 2005, in *The Astrophysics of Cataclysmic Variables and Related Objects*, edited by J.-M. Hameury, J.-P. Lasota, vol. 330 of *Astronomical Society of the Pacific Conference Series*, 147
- Nardini E., Fabian A. C., Reis R. C., Walton D. J., 2011, *MNRAS*, 410, 1251
- Neilsen J., Lee J. C., 2009, *Nat*, 458, 481
- Oliva E., Marconi A., Moorwood A. F. M., 1999, *A&A*, 342, 87
- Piconcelli E., Cappi M., Bassani L., Di Cocco G., Dadina M., 2003, *A&A*, 412, 689
- Ponti G., Fender R. P., Begelman M. C., Dunn R. J. H., Neilsen J., Coriat M., 2012, *MNRAS*, 422, L11
- Portegies Zwart S. F., Baumgardt H., Hut P., Makino J., McMillan S. L. W., 2004, *Nat*, 428, 724
- Poutanen J., Lipunova G., Fabrika S., Butkevich A. G., Abolmasov P., 2007, *MNRAS*, 377, 1187
- Ptak A., Colbert E., van der Marel R. P., Roye E., Heckman T., Towne B., 2006, *ApJS*, 166, 154
- Raymond J. C., Smith B. W., 1977, *ApJS*, 35, 419
- Reis R. C., Fabian A. C., Miller J. M., 2010, *MNRAS*, 402, 836
- Reis R. C., Miller J. M., 2013, *ApJ*, 769, L7
- Reis R. C., Miller J. M., Fabian A. C., 2009, *MNRAS*, 395, L52
- Reis R. C., Miller J. M., Fabian A. C., et al., 2011, *MNRAS*, 410, 2497
- Remillard R. A., McClintock J. E., 2006, *ARA&A*, 44, 49
- Reynolds M. T., Miller J. M., 2013, *ApJ*, 769, 16
- Risaliti G., Harrison F. A., Madsen K. K., et al., 2013, *Nat*, 494, 449
- Rivers E., Markowitz A., Rothschild R., 2013, *ArXiv e-prints*
- Roberts T. P., 2007, *Astrophysics and Space Science*, 311, 203
- Ross R. R., Fabian A. C., 2005, *MNRAS*, 358, 211
- Saito K., Yamaoka K., Fukuyama M., Miyakawa T. G., Yoshida A., Homan J., 2006, in *VI Microquasar Workshop: Microquasars and Beyond*
- Sale S. E., Drew J. E., Knigge C., et al., 2010, *MNRAS*, 402, 713
- Salvesen G., Miller J. M., Reis R. C., Begelman M. C., 2013, *MNRAS*, 431, 3510
- Servillat M., Farrell S. A., Lin D., Godet O., Barret D., Webb N. A., 2011, *ApJ*, 743, 6
- Shakura N. I., Sunyaev R. A., 1973, *A&A*, 24, 337
- Shimura T., Takahara F., 1995, *ApJ*, 445, 780
- Steiner J. F., Narayan R., McClintock J. E., Ebisawa K., 2009, *PASP*, 121, 1279
- Stern D., Eisenhardt P., Gorjian V., et al., 2005, *ApJ*, 631, 163
- Stobart A.-M., Roberts T. P., Wilms J., 2006, *MNRAS*, 368, 397
- Strohmer T. E., 2009, *ApJ*, 706, L210
- Strüder L., Briel U., Dennerl K., et al., 2001, *A&A*, 365, L18
- Sutton A. D., Roberts T. P., Gladstone J. C., et al., 2013, *ArXiv e-prints*
- Sutton A. D., Roberts T. P., Walton D. J., Gladstone J. C., Scott A. E., 2012, *MNRAS*, 423, 1154
- Swartz D. A., Ghosh K. K., Tennant A. F., Wu K., 2004, *ApJS*, 154, 519
- Swartz D. A., Soria R., Tennant A. F., Yukita M., 2011, *ApJ*, 741, 49
- Tao T., Blaes O., 2013, *ApJ*, 770, 55
- Titarchuk L., 1994, *ApJ*, 434, 570
- Tomsick J. A., Yamaoka K., Corbel S., Kaaret P., Kalemci E., Migliari S., 2009, *ApJ*, 707, L87
- Torrejón J. M., Schulz N. S., Nowak M. A., Kallman T. R., 2010, *ApJ*, 715, 947
- Tsujimoto M., Guainazzi M., Plucinsky P. P., et al., 2011, *A&A*, 525, A25
- Turner M. J. L., Abbey A., Arnaud M., et al., 2001, *A&A*, 365, L27
- Vaughan S., Fabian A. C., Nandra K., 2003, *MNRAS*, 339, 1237
- Walton D. J., Gladstone J. C., Roberts T. P., et al., 2011a, *MNRAS*, 414, 1011
- Walton D. J., Miller J. M., Harrison F. A., et al., 2013a, *ArXiv e-prints*
- Walton D. J., Miller J. M., Reis R. C., Fabian A. C., 2012a, *MNRAS*, 426, 473
- Walton D. J., Nardini E., Fabian A. C., Gallo L. C., Reis R. C., 2013b, *MNRAS*, 428, 2901
- Walton D. J., Reis R. C., Cackett E. M., Fabian A. C., Miller J. M., 2012b, *MNRAS*, 422, 2510
- Walton D. J., Reis R. C., Fabian A. C., 2010, *MNRAS*, 408, 601
- Walton D. J., Roberts T. P., Mateos S., Heard V., 2011b, *MNRAS*, 416, 1844
- Watarai K., Mizuno T., Mineshige S., 2001, *ApJ*, 549, L77
- Weisskopf M. C., Brinkman B., Canizares C., Garmire G., Murray S., Van Speybroeck L. P., 2002, *PASP*, 114, 1
- Werner M. W., Roellig T. L., Low F. J., et al., 2004, *ApJS*, 154, 1
- Williams M. J., Bureau M., Cappellari M., 2010, *MNRAS*, 409, 1330
- Wilms J., Allen A., McCray R., 2000, *ApJ*, 542, 914
- Winter L. M., Mushotzky R. F., Reynolds C. S., 2006, *ApJ*, 649, 730
- Zampieri L., Roberts T. P., 2009, *MNRAS*, 400, 677
- Zdziarski A. A., Poutanen J., Paciesas W. S., Wen L., 2002, *ApJ*, 578, 357